Journal of Functional Foods 133 (2025) 107002

Contents lists available at ScienceDirect

Journal of Functional Foods

journal homepage: www.elsevier.com/locate/jff

Exploring by-products as sources of bioactive compounds: LC-ESI-QTOF-MS profiling and bioactivity assessment of blood twig dogwood and cornelian cherry leaf extracts and fractions

Maria Concetta Tenuta [a], Brigitte Deguin [b,*], Monica Rosa Loizzo [c], Fedora Grande [c], Matteo Brindisi [d], Maria Antonietta Occhiuzzi [c], Annabelle Dugay [b], Marco Bonesi [c], Giuseppe Antonio Malfa [e], Rosa Tundis [c,*]

[a] Faculty of Agricultural, Environmental and Food Science, Free University of Bozen-Bolzano, Piazza Università 1, 39100 Bolzano, Italy
[b] Université Paris Cité, Faculté de Pharmacie de Paris, U.M.R. n°8038, -CïTCoM- (CNRS, Université Paris Cité), F-75006 Paris, France
[c] Department of Department of Pharmacy, Health and Nutritional Sciences, University of Calabria, Rende (Cosenza), Italy
[d] IRCCS Humanitas Research Hospital, Milan, Italy
[e] Department of Drug Science - Biochemistry Section, University of Catania, Viale A. Doria 6, 95125 Catania, Italy

ARTICLE INFO

Keywords:
LC-ESI-QTOF-MS
Cornus sanguinea
Cornus mas
Sweroside
Cornuside
Bioactivity
Molecular docking

ABSTRACT

The increasing incidence of chronic diseases, interest in bioactive compounds from agro-industrial by-products is increasing. This study explored the chemical profile and bioactivities of *Cornus mas* and *Cornus sanguinea* leaf extracts obtained through various extraction methods, especially focusing on the lesser-known *C. sanguinea*. The study assessed their anti-inflammatory properties (inhibition of NF-κB, nitric oxide reduction), antioxidant activity, and hypoglycaemic effects (inhibition of α-amylase and α-glucosidase). LC-ESI-QTOF-MS analysis identified phenolic acids, iridoids, and flavonoids as key constituents. Hydroalcoholic maceration of dried *C. mas* and ethanol maceration of fresh *C. sanguinea* were fractionated using XAD-16 resin. Bioactivity was tested on fractions and on three key compounds: sweroside, cornuside, and ellagic acid. Sweroside and cornuside inhibited highly NO production. Moreover, sweroside exhibited a notable α-glucosidase inhibition. These findings highlight the potential benefits of *Cornus* leaves, providing a basis to develop *Cornus*-based products for the prevention or treatments for type 2 diabetes and inflammation.

1. Introduction

The genus *Cornus* (Cornaceae family) consists of about 65 species that are mostly trees and shrubs with woody rhizomes, widely distributed in the northern hemisphere with centers of diversity in southern and central Europe, southwest Asia, mountains of Central America, eastern and western North America, east Africa and South America (Tenuta et al., 2022).

Cornus mas L. (commonly known as Cornelian cherry) is a deciduous shrub or small tree used for centuries in various countries of Europe and Asia not only as food but also in traditional medicine for the prevention and treatment of a wide range of diseases including diabetes, kidney and liver diseases, infections, gastrointestinal disorders, and rheumatic pain. The referred studies of biological activity indicated the antioxidant, hepatoprotective anti-inflammatory, antibacterial, antidiabetic, hypolipidemic, and anticancer properties (Lidiková et al., 2024; Sevindik

Abbreviations: ABTS, 2,2′-azino-bis(3-ethylbenzothiazoline-6-sulfonic acid) diammonium salt; ADMET, Absorption, Distribution, Metabolism, Excretion, and Toxicity; BHT, Butylated hydroxytoluene; COX-2, Cyclooxygenase-2; CtMGAM, Carboxy-terminal active domain; DIAN, *o*-Dianisidine; DMEM, Dulbecco's modified Eagle's medium; FRAP, Ferric Reducing Antioxidant Power; HFF1, Human Foreskin Fibroblasts; IC_{50}, Half maximal inhibitory concentration; ICAM-1, Intercellular Adhesion Molecule 1; IL-2, Interleukin-2; iNOS, Inducible nitric oxide synthase; LC-ESI-QTOF-MS, Liquid chromatography-electrospray ionization-quadrupole-time of mass spectrometry; LE, Ligand efficiency; LPS, Lipopolysaccharides; MTT, 3-(4,5-dimethyl-2-thiazolyl)-2,5-diphenyl-2H-tetrazolium bromide; NF-κB, Nuclear factor kappa-light-chain-enhancer of activated B cells; NO, Nitric oxide; PGO, Peroxidase-glucose oxidase; ROS, Reactive oxygen species; SD, Standard deviation; TBS, Tris Buffer Saline; VCAM-1, Vascular Cell Adhesion Molecule 1.

* Corresponding authors.
E-mail addresses: brigitte.deguin@u-paris.fr (B. Deguin), rosa.tundis@unical.it (R. Tundis).

https://doi.org/10.1016/j.jff.2025.107002
Received 15 April 2025; Received in revised form 8 July 2025; Accepted 25 August 2025
Available online 4 September 2025

et al., 2024).

Cornus sanguinea L. (also known as blood twig dogwood or common dogwood) is a small tree with leaves with a characteristic dark red colour in senescence. It has been traditionally used in Turkey to treat diarrhoea and gastrointestinal disorders, and in Italy as an astringent. In contrast to *C. mas*, there is limited research available on this *Cornus* species (Hozoori et al., 2012; Iannuzzi et al., 2021; Stanković & Topuzović, 2012).

Until now, great attention has been given to the fruits. However, the leaves of *Cornus mas* and *C. sanguinea* may represent by-products that could be serve as a valuable natural source of bioactive compounds. Indeed, several chemical investigations have identified phenolic compounds (including flavonoids) and iridoids as the main classes of secondary metabolites of both species (Dinda et al., 2016; Szczepaniak et al., 2019; Tenuta et al., 2022). Among these phytochemicals, phenolic compounds are one of the classes of bioactive secondary metabolites most studied and with well-reported health benefits on human health including protection against cancer, diabetes, osteoporosis, and neurological and cardiovascular diseases (Cory et al., 2018; Rahman et al., 2022). These beneficial effects are partly due to their ability to act as potent antioxidants, as scavengers of reactive oxygen species (ROS), produced under oxidative stress conditions and during inflammatory and degenerative diseases (Durazzo et al., 2019; Mark et al., 2019). These properties suggest the potential use of natural phenolic compounds in the food industry as food additives, as well as for biomedical and cosmetic applications.

Recently, another class of natural compounds that shown promising health effects, such as antioxidant, anti-inflammatory, antitumor, neuroprotective, and hypoglycaemic properties, is represented by the cyclopentane[*c*]pyran monoterpenoids iridoids (Kandar, 2021; Wang et al., 2020). Iridoids, which can be divided into 4 groups, namely iridoid glycosides, non-glycosidic iridoids, secoiridoid glycosides, and bis-iridoids, are prevalent in dicotyledonous plants from Gentianaceae, Labiatae, Scrophulariaceae, Oleaceae, Pyrolaceae, and Rubiaceae.

Bioactive compounds are generally found in fruits but also in other under-valorised sources such as the agri-industrial by-products and considered a worldwide issue that negatively impact on environmental system due to the current unsuitable management. Indeed, a high quantity of by-products (such as leaves) is produced in food processing. This represents a problem because around 1.13 million tons of food waste are discarded globally every day (Chen et al., 2020). In Europe, over 58 million tons of food waste (131 kg/inhabitant) are generated every year, with a corresponding estimated market value of 132 billion euros (Eurostat, 2023; Yadav et al., 2024).

Many governments are moving towards a more sustainable approaches, implementing the ambitious circular economy plan with the main goal of reducing, and encouraging the adequate reuse of an unexploited sources of valuable compounds such as agri-food by-products (e.g., leaves). Thus, the recovery of bioactive compounds from by-products can provide an additional economic value (Messinese et al., 2024).

In this context, this study investigated the potentiality of *C. mas* and *C. sanguinea* as valuable source of bioactive compounds useful to treat type 2 diabetes and inflammation. With this aim, we prepared extracts by using different extraction procedures and solvent systems and we employed amberlite XAD-16 resin to obtain fractions enriched in flavonoids and iridoids. This approach could offer an alternative to traditional separation methods, reducing solvent consumption, processing time, chemical residues and operational costs (Fredsgaard et al., 2023). Advancing research in this area, alongside the development of innovative extraction and fractionation methods, could promote the sustainable valorisation of these plant resources, minimizing waste while enhancing their potential applications for the production of pharmaceutical products and functional foods.

2. Materials and methods

2.1. Chemicals and reagents

Solvents used for liquid chromatography-electrospray ionization-quadrupole-time of flight-mass spectrometry (LC-ESI-QTOF-MS) were purchased from Carlo Erba s.r.l. (Milan, Italy). Loganin, ferulic acid, and hyperoside were purchased from Extrasynthese (Lyon, France). XAD-16 resin was purchased from Alfa-aesar, Thermo Fisher Scientific (Kandel, Germany). The anti-NF-κB p65 monoclonal antibody was purchased from Santa Cruz Biotechnology (CA, USA). Murine macrophages RAW 264.7 cells were obtained from American type culture collection (VA, USA). Solvents used for analytical analyses were obtained from VWR International s.r.l. (Milan, Italy). Aucubin, chlorogenic acid, ascorbic acid, cornuside, ellagic acid, gallic acid, isoquercitrin, quercetin, quinic acid, rutin, propyl gallate, syringic acid, acetic acid, butylated hydroxytoluene (BHT), 2,2′-azino-bis(3-ethylbenzothiazoline-6-sulfonic acid) diammonium salt (ABTS) solution, β-carotene, 2,4,6-tri(2-pyridyl)-*s*-triazine (TPTZ), *α*-amylase from porcine pancreas (EC 3.2.1.1), dimethyl sulfoxide (DMSO), *α*-glucosidase from *Saccharomyces cerevisiae* (EC 3.2.1.20), Griess reagent, 3-(4,5-dimethyl-2-thiazolyl)-2,5-diphenyl-2H-tetrazolium bromide (MTT), interleukin-2 (IL-2), Folin-Ciocalteu reagent, sodium nitrite, aluminum chloride, sodium hydroxide, potato starch, linoleic acid, Tween 20, 3,5-dinitrosalicylic acid, maltose, sodium potassium tartrate, *o*-dianisidine (DIAN), lipopolysaccharides (LPS), sodium carbonate, 6-hydroxy-2,5,7,8-tetramethylchroman-2-carboxylic acid (Trolox), peroxidase-glucose oxidase (PGO), sodium phosphate, Tris Buffer Saline (TBS), bovine serum albumin, sodium chloride, fetal bovine serum, Dulbecco's modified Eagle's medium (DMEM), Eagle's minimum essential medium (EMEM), glucose, penicillin-streptomycin, sodium acetate, IgG-TRITC, were purchased from Sigma-Aldrich s.r.l (Milan, Italy). Acarbose from *Actinoplanes* sp. was purchased from Serva (Heidelberg, Germany). L-N6-(1-iminoethyl) lysine and IgG-TRITC were purchased from ThermoFisher Scientific (Waltham, MA, USA).

2.2. Plant materials and extraction procedures

The leaves of *Cornus sanguinea* were harvested in the Botanic Garden of the University of Calabria (Rende, Italy) at the maturity stage of the fruits (WGS84: 39°24′33″ N, 16°13′43″ E) (plant n. 165). The leaves of *Cornus mas* were harvested in the "Parco della Cessuta", Cerchiara di Calabria (Cosenza, Italy) (WGS84: 39°51′41″ N, 16°21′47″ E) (Voucher n. CLU262579 at the maturity stage of fruits. Prof. N.G. Passalacqua (University of Calabria, Italy) carried out the botanical authentication of samples.

Leaves of both *Cornus* species were divided in two parts: one part was extracted immediately, while the other one was dried at room temperature for 7 days in the dark. The following extraction procedures were applied: a) maceration with ethanol (EtOH) as solvent (n. 3 extractions, each of 72 h); b) maceration with hydroalcoholic ethanol solution (60 % *v/v*, (n. 3 extractions, each of 72 h); c) ultrasound-assisted extraction (ethanol, n. 3 cycles, each of 1 h) using a Branson 3800 ultrasonic system, series CPXH (130 W, 40 kHz frequency) (Milan, Italy); d) decoction (water, 100 °C, 30 min).

Extraction yields (expressed as g dried extract/g plant materials × 100) are reported in Tables S1 and S2 (Supplementary Materials).

2.3. Total phytochemicals (iridoids, phenols, and flavonoids) content

C. sanguinea and *C. mas* extracts were tested for their total content of iridoids, phenols, and flavonoids. The total iridoid content (TIC) was determined according to a method based on the Trim and Hill reaction in which the extract (400 μL, concentration of 1.5 mg/mL) was mixed with the Trim-Hill reagent (4.0 mL, acetic acid/0.2 % $CuSO_4$/HClaq, 10:1:0.5 *v/v/v*).

After heating at 100 °C for 5 min, the absorbance was read at 609 nm using a UV–vis Jenway 6003 spectrophotometer (Milan, Italy). TIC was determined in triplicate and expressed as milligrams of aucubin equivalents (AU) The Folin-Ciocalteu reagent was used to assess the total phenol content (TPC). In brief, 100 μL of extract (1.5 mg/mL) was mixed with 2 mL of water, 1 mL of sodium carbonate 15 % (*w/v*) aqueous solution, and 0.2 mL of Folin-Ciocalteu reagent. After incubation (2 h) at 25 °C, the absorbance was measured at 765 nm. TPC was determined in triplicate and expressed as milligrams of chlorogenic acid equivalents (CA)/g of extract.

The total flavonoid content (TFC) was determined using a method that involves the formation of a complex between aluminum ions and flavonoids, which can be measured spectrophotometrically. Briefly, 1 mL of extract (1.5 mg/mL) was added to 0.3 mL of 5 % (w/v) sodium nitrite and 4 mL of distilled water. After 5 min, 0.6 mL of 10 % (w/v) aluminum chloride was added, and 6 min later, 2 mL of 1 M sodium hydroxide and 2.1 mL of distilled water were added. Absorbance was read at 510 nm. The total flavonoids content was determined in triplicate and expressed as milligrams of quercetin equivalents (QE)/g of extract.

2.4. Liquid chromatography-electrospray ionization-quadrupole-time of flight-mass spectrometry (LC-ESI-QTOF-MS) analyses of extracts

The chemical composition of *C. mas* and *C. sanguinea* leaf extracts was analysed by using an HPLC (U-3000, Thermo, Courtaboeuf, France) coupled to an ESI-QTOF mass spectrometer (Maxis II, Bruker, Champs sur Marne, France) as previously described with some modification (Tenuta et al., 2020). The chromatographic separation was achieved on a C18 column (Acclaim RSLC polar advantage II, 100 × 2.1 mm, 2.2 mm) at a temperature of 35 °C, with a speed of flow of 0.3 mL/min. The mobile phase consisted of a mixture of 0.1 % formic acid, 10 % methanol and water (phase A), and 0.1 % formic acid and acetonitrile (phase B). The elution gradient was as follows: 0 to 2 min 95 % A; 2 to 7 min, 95 to 85 % A; 7 to 15 min, from 85 to 50 % A; 15 to 18 min, 50 to 20 % A; 18 to 19 min, 20 % and 19 to 21 min, 20 to 95 % A. The injection volume was 2 μL and the flow rate was 0.3 mL/min. Chromatograms were acquired at four different wavelengths namely 240, 280, 340, and 510 nm. The mass spectra were obtained in positive mode by using the following parameters: ESI 3500 V, *m/z* 50–1200, MS 2 Hz. Comparison with UV spectra and molecular weight (*m/z* ion $[M + H]^+$ or $[M + Na]^+$) were used for identification of constituents. Authentic standards were used to confirm the presence of chlorogenic acid, cornuside, sweroside, ellagic acid, ferulic acid, gallic acid, hyperoside, isoquercitrin, quercetin, quinic acid, rutin, and syringic acid.

2.5. Fractionation process

Amberlite XAD-16 resin was used obtain fractions enriched in flavonoids and iridoids from A1 sample (ethanol maceration of *C. sanguinea* fresh leaves) and D2 sample (hydroalcoholic maceration of *C. mas* dried leaves) (Tomás-Barberán et al., 1992). These extracts exhibited not only the most promising hypoglycaemic activity through the inhibition of α-glucosidase with IC_{50} values lower than that reported for the positive control acarbose, but also the best radical scavenging activity and inhibition of lipid peroxidation.

XAD-16 is a neutral resin formed of an aliphatic polymer cross-linked macroreticular, recommended for the adsorption of phenols from aqueous solvents. The chemical and physical properties of the resin are dry density (vs. wet) of 1.08 (1.02) g/mL, surface area of 900 sq. m/g, pore diameter of 100 Angstroms, west mesh size (nominal) from 20 to 60, and pore volume of 1.82 mL/g. Its structure approves adsorbing organic molecules with a molecular weight from rather low to medium. XAD-16 resin was activated 24 h by using methanol (160 mL). Methanol was replaced by water before starting the adsorption procedure. Then, extract A1 (4 g) and extract D2 (4 g) were dissolved in distilled water (a preliminary step with ethanol was required only for A1 to completely dissolve the extract), placed on resin into a glass bottle and shaken for 30 min. After each elution of 15 min, the resin was filtered.

The following sequential elution was applied: 840 mL of water, 420 mL of 80 % ethanol, and 700 mL of absolute ethanol. Fractions were evaporated under reduced pressure and analysed by LC-MS. The chemical composition of fractions, obtained after separation on XAD-16 resin, was analysed through LC-MS. The HPLC system Thermo Scientific Dionex UltiMate 3000 Series with DAD and MS simple quadrupole (MSQ plus-Surveyor) detections (Courtabœuf, France) comprised a vacuum degasser, a quaternary pump, an automatic sampler and a PDA spectrophotometer detector, that detects at 210, 240, 280 and 340 nm and between 200 and 600 nm. A column C18 (Acclaim Polar Advantage II (Thermo Scientific, Courtabœuf, France), 100 × 2.1 mm, 3 μm) was selected and thermostated at 35 °C. The flow rate was set at 0.5 mL/min; the sample injection volume was 10 μL. The solvents used were: solvent A: 0.1 % formic acid in ultrapure water containing 10 % LC-MS grade methanol (*v/v*), solvent B: 0.1 % formic acid in acetonitrile LC-MS grade (*v/v*). At the injection time and for 2 min, the volume *ratio* A:B was set at 100:0. Then, elution profile was 95:5 (A:B) from 2 to 5 min, 80:20 (A:B) from 5 to 20 min, 60:40 (A:B) from 20 to 25 min, and 20:80 (A:B) from 25 to 30 min. This last *ratio* is maintained and returned to the initial condition from 33 to 36 min.

The chromatographic effluent stream was directed into the mass spectrometer (MS) interface that consisted of an electrospray ionization (ESI) source, in positive and/or negative ionization mode. The conditions are as follows: capillary voltage was set at 3 kV, the flows of nebulizing and drying gas (nitrogen) were respectively set at 9.0 L/min and 4.0 bar and drying gas was heated at 500 °C, generated by a nitrogen generator (F DGSi Alliance Innovation Gas System Company). Mass spectra were obtained in the range 100–1300 Thomson where the cone energy is 50 V in scanning mode. The ions produced are formed by collision-induced dissociation (CID). For data treatment was used the software Chromeleon 6.8, provided by Thermo Scientific (91,940 Les Ulis, France).

2.6. Inhibition of carbohydrate hydrolysing enzymes

The α-glucosidase and α-amylase inhibition assays were used to investigate the potential hypoglycaemic activity of *Cornus* leaves extracts and pure compounds (Loizzo et al., 2016).

The inhibition of these enzymes involved in the digestion of carbohydrates can reduce the post-prandial increase of blood glucose and therefore can be an important strategy in the management of blood glucose levels in type 2 diabetic and borderline patients.

In the α-glucosidase inhibition test, extracts and fractions (at concentrations in the range 1–1000 μg/mL) and pure compounds (at concentrations in the range 1–50 μg/mL) were added to maltose solution and left to equilibrate at 37 °C for 5 min. The reaction was activated through add of α-glucosidase solution and left to incubate at 37 °C for 30 min. Perchloric acid solution (0.7 % *v/v*) was used to lock the reaction. The supernatant (centrifugation for 5 min at 3000*g*) was collected and mixed with peroxidase/glucose oxidase and *o*-dianisidine and left to incubate for 30 min at 37 °C. The absorbance was spectrophotometric measured at 500 nm (UV–Vis Jenway 6003 spectrophotometer, Carlo Erba, Milan, Italy).

In the α-amylase inhibition test, the colorimetric reagent (3,5-dinitrosalicylic acid) solution, α-amylase solution, and starch solution were prepared. Extracts and fractions (at concentrations in the range 1–1000 μg/mL) and pure compounds (at concentrations in the range 1–50 μg/mL) were mixed with starch solution and left to react with α-amylase solution at room temperature for 5 min. The quantity of maltose was measured at 540 nm through the reduction of 3,5-dinitrosalicylic acid to 3-amino-5-nitrosalicylic acid. The commercial drug acarbose was used as positive control in both tests.

2.7. Molecular docking studies on carbohydrate digestive enzymes

Molecular docking of cornuside, ellagic acid, and sweroside was performed on the crystallographic structure of the human carboxy-terminal active domain (CtMGAM) of α-glucosidase and human pancreatic α-amylase obtained from the Protein Data Bank (PDB) and corresponding to entries 3TOP and 4 W93, respectively (Ren et al., 2011; Williams et al., 2015).

In particular, the α-glucosidase is complexed with the crystallographic ligand acarbose (AC1) and the α-amylase with its known inhibitor montbretin A (3 L9) a. The molecular structure of the ligand was built by using the modeling software Avogadro (Hanwell et al., 2012). Docking calculations were performed by using AutoDockVina1.1.2 (Trott & Olson, 2010).

Preliminary conversion of the structures from the PDB format was carried out by using the graphical interface Auto Dock Tools 1.5.6, polar hydrogens were added for the crystallographic enzymes, and apolar hydrogens of all compounds were merged to the carbon atom they were attached to (Morris et al., 1998). Full flexibility was guaranteed for the ligands, resulting in 18, 4 and 8 rotatable dihedral angles for cornuside, ellagic acid and sweroside, respectively. A single simulation run was carried out in each case at very high exhaustiveness, 16 times larger than the default value (Cirillo et al., 2024). The binding modes of the ligand were analysed through visual inspection by using VMD (Humphrey et al., 1996).

The Molecular Graphics System PyMOL has been used to visualise protein structure. Ligand binding intermolecular interactions were evaluated using the automated protein–ligand interaction profiler (PLIP) (Adasme et al., 2021).

Additionally, the inhibition constant (Ki) was calculated based on the binding energy according to the following equation:

$$\Delta G = RT\ln(Ki)$$

whereas ΔG, R, and T are related to the binding energy (kcal/mol), gas constant (1.987 cal/K mol), and temperature (310.15 K) (Shahraki et al., 2024; Taghizadeh et al., 2022).

Finally, the ligand efficiency was calculated according to the following equation:

$$LE = -\Delta G/Nnon - H$$

whereas Nnon-H corresponds to the number of non-hydrogen atoms (Kenny, 2019).

2.8. ADMET properties of studied compounds

The pharmacokinetic and drug-likeness properties of cornuside, ellagic acid and sweroside were evaluated using the SwissADME server (http://www.swissadme.ch/) using the SMILES representation of the molecules. Several characteristics including solubility, lipophilicity, bioavailability score, blood-brain barrier permeability, skin permeability (LogKP), gastrointestinal absorption and compliance with the rules of Lipinski, Ghose, Veber, Egan and Muegge were calculated (Lotfi et al., 2025; Shahraki et al., 2024).

2.9. Cell culture

The human foreskin fibroblast cell line HFF-1 (ATCC® SCRC-1041.1) was cultured in DMEM supplemented with 15 % (*v*/v) fetal bovine serum (FBS), 4.5 g/L glucose, 100 U/mL penicillin, and 100 μg/mL streptomycin. These cells were used as an in vitro human model for preliminary toxicity screening. Additionally, HFF-1 cells were employed to evaluate the anti-inflammatory effects of the extracts using an interleukin-2β-induced inflammation model in vitro. Mouse macrophage RAW 264.7 cells (Sigma-Aldrich 91062702) were maintained in EMEM supplemented with 2 mM L-glutamine, 1 % non-essential amino acids, 10 % FBS, and antibiotics including penicillin, streptomycin, and amphotericin. RAW 264.7 cells served as an in vitro model to study inflammation induced by lipopolysaccharide (LPS).

2.10. Cell viability assay

HFF-1 and RAW 264.7 cells were seeded under sub-confluent conditions at a constant density of 8×10^3 cells/well to ensure consistent experimental conditions across the different assays and to improve the accuracy of the measurements. Cell metabolic activity was assessed using the 3-(4,5-dimethyl-2-thiazolyl)-2,5-diphenyl-2H-tetrazolium bromide (MTT) assay. This assay measures cell viability based on the ability of metabolically active cells to convert the yellow tetrazolium salt (MTT) into insoluble purple formazan crystals (Davì et al., 2023). The amount of formazan produced, which is directly proportional to the number of viable cells, was quantified spectrophotometrically at 570 nm. Results were expressed as the percentage of cell viability relative to the untreated control group.

2.11. Inhibition of nitric oxide (NO) production

The inhibition of nitric oxide (NO) production by the extracts was evaluated using the Griess reagent method (Davì et al., 2023). HFF-1 cells were pre-treated with the different concentrations of extract (2.5, 12.5, and 25 μg/mL) for 90 min, followed by stimulation with interleukin-2β (IL-2β) at a concentration of 10 μg/mL for 30 min. In contrast, RAW 264.7 cells were pre-treated with the different concentrations of extract (2.5, 12.5, and 25.0 μg/mL) for 24 h, followed by stimulation with lipopolysaccharide (LPS) at 1 μg/mL for 2 h.

To quantify NO production, 250 μL of Griess reagent was added to 250 μL of culture medium, and the total nitrite concentration was measured spectrophotometrically at 546 nm. Results were expressed as the mean IC_{50} (μg/mL), representing the concentration required to reduce nitrite production by approximately 50 %. L-N^6-(1-iminoethyl) lysine (L-NIL) at 1 μg/mL was used as a positive control for NO inhibition, known to reduce inducible nitric oxide synthase (iNOS) activity by approximately 50 %.

2.12. Inhibition of NF-κB pathway in LPS-stimulated RAW 264.7 cells

RAW 264.7 macrophages were spread on coverslip at 1×10^5 density and cultured overnight in the complete medium; then, they were treated with LPS (1 μg/mL) and fraction for 1 h at their half-maximal inhibitory concentration (IC_{50}) value. Cells were washed twice in PBS and then ice-cold methanol was used to fix cells for 20 min at −20 °C. Cells were washed with Tris buffer saline (TBS) and incubated for blocking with 5 % bovine serum albumin in TBS for 40 min at 37 °C (Brindisi et al., 2021). Then, cells were incubated in anti-NF-κB p65 monoclonal antibody diluted 1:200, for 40 min at 37 °C, washed with TBS, and incubated in anti-mouse IgG-TRITC, diluted 1:300, for 40 min at 37 °C in TBS. Finally, cells were washed with TBS before microscope visualisation. Images at 20× magnification were acquired under an Olympus BX41 microscope with CSV1.14 software, by using a CAMXC-30 for image acquisition.

2.13. In vitro antioxidant activity

Oxidative stress plays an important role in the pathogenesis of several chronic diseases including cancer, diabetes, and cardiovascular and neurodegenerative diseases. Besides the well-known and traditionally used natural antioxidants from fruits, vegetables and spices (e.g. wine, red fruits, tea) many other plant species have been investigated in the search for new antioxidants. Some natural antioxidants (e.g. sage and rosemary) are already used commercially either as antioxidant additives or as nutritional supplements. Measuring the antioxidant activity of a sample is therefore crucial in studying the efficiency of an

antioxidant molecule in preventing and/or treating diseases related to oxidative stress such as type 2 diabetes. There are several methods available for measuring antioxidant activity. Herein, the antioxidant effects of *Cornus* extracts, fractions and pure compounds were evaluated by using three assays namely 2,2′-azino-bis(3-ethylbenzothiazoline-6-sulfonic acid) (ABTS) test, *β*-carotene bleaching test, and Ferric Reducing Antioxidant Power (FRAP) test.

2.13.1. ABTS test

Currently, there is growing interest in antioxidants, particularly for preventing the well-known harmful effects of free radicals in human metabolism and during processing and storage of fatty foods. Therefore, there has been an increase in the use of tests to assess antioxidant efficacy in both human metabolism and food systems. Today, there are many bioanalytical methods that measure the antioxidant effect. Of these, the ABTS assay is a widely used method for determining antioxidant activity, known for its technical simplicity and ability to measure both lipophilic and hydrophilic antioxidant compounds. In brief, a solution of ABTS radical cation ($ABTS^{+}$, 2 mM) was mixed to potassium persulphate (70 mM) (Meringolo et al., 2022). After 12 h, the solution was diluted with ethanol to an absorbance of 0.70 ± 0.03 and measure at 734 nm using a UV–Vis Jenway 6003 spectrophotometer (Carlo Erba, Milan, Italy). The absorbance of a mixture of extracts and fractions (at concentration ranging from 400 to 1 μg/mL), pure compounds (at concentration ranging from 10 to 0.15 μg/mL), and $ABTS^{+}$ solution was read after 6 min. The ABTS scavenging ability was calculated as follows: ABTS scavenging activity (%) = $[(A_0 - A)/A_0] \times 100$, where A_0 is the absorbance of the control reaction and A is the absorbance in the presence of extract. Ascorbic acid was used as positive control.

2.13.2. β-Carotene bleaching test

Lipid peroxidation can be defined as a process in which oxidants such as free radicals attack lipids containing carbon-carbon double bond/bonds. In recent decades, a substantial body of literature has highlighted the critical role of lipid peroxidation in cell biology and human health.

Indeed, lipid peroxidation can lead to cell membrane damage, protein and DNA modification. Inhibiting this process is crucial for maintaining cellular health and preventing disease progression. To assess the ability of *Cornus* samples to inhibit lipid peroxidation, the β-carotene bleaching test was carried out according to the method previously described (Meringolo et al., 2022). The test was carried out at the initial time ($t = 0$) and after 30 and 60 min of incubation. a mixture of linoleic acid (20 μL), Tween 20 (100 %, 200 μL) and β-carotene (1 mL) was prepared. After evaporation of solvent at 40 °C and dilution with water (100 mL), the emulsion was added into the tubes (288 μL) containing samples or fractions at different concentration (100–1 μg/mL) or pure compounds (at concentrations in the range 1–40 μg/mL) and incubated at 45 °C for 30 and 60 min. Propyl gallate was used as a positive control. The absorbance was measured at 470 nm. The antioxidant activity (A) was calculated by using the following equation: $A = [(A_0 - A_t)/(A_0^{\#} - A_t^{\#})] \times 100$, where A_0 and $A_0^{\#}$ are the absorbance values at time 0 for the samples and control, respectively, while A_t and $A_t^{\#}$ are the absorbance values after 30 and 60 min of incubation for the samples and controls, respectively.

2.13.3. FRAP test

FRAP test is a simple and sensitive method that measures the reduction of the complex of ferric ions (Fe^{3+})-ligand to the intensely blue ferrous complex (Fe^{2+}) by means of antioxidants in acid environments (Meringolo et al., 2022). For the preparation of FRAP reagent a mixture of 2.5 mL of 10 mM tripyridyltriazine (TPTZ) solution in 40 mM HCl, 2.5 mL of 20 mM $FeCl_3$ and 25 mL of 0.3 M acetate buffer (pH 3.6) was prepared. A mixture of 0.2 mL of samples (at concentrations of 2.5 mg/mL for extracts and 1.0 mg/mL for fractions and pure compounds) and 1.8 mL of FRAP reagent was prepared. The absorbance of the reaction mixture was measured at 595 nm after 30 min of incubation at room temperature. FRAP value was expressed as μM Fe(II)/g. Butylated hydroxytoluene (BHT) was used as a positive control.

2.14. Statistical analysis

Values are expressed as mean ± standard deviation (SD) of the mean. Results are treated through statistical procedures to evidence any significant relationship between the chemical composition of the extracts and/or fractions and bioactivity. Data are subjected to a One-way analysis of variance (ANOVA) and the significance of the differences between groups with the positive control were determined by multi-comparison Dunnett's test (p value <0.05) using Graphpad Prism 4 statistical software package (Graphpad, San Diego, CA, USA).

3. Results and discussion

3.1. Chemical study

The fresh and dried leaves of *C. sanguinea* and *C. mas* were extracted by applying different procedures such as maceration, decoction, and ultrasound-assisted extraction (UAE) to evaluate which extraction method can be used to achieve the highest yield of active compounds.

Maceration is a common solid-extraction method that involves selecting the polarity of the solvent. Compared to other procedures, it can be done with simple-to-use equipment and low-cost. Moreover, it can be customized to extract a wide diversity of molecules by combining different solvents and agitation to promote a more selective and effective mass transfer of high-value chemicals from biomass. The main disadvantages of this extraction technique are the extended extraction times and high amounts of solvent used. Water decoction is a widely used technique in traditional medicine, particularly in systems like Traditional Chinese Medicine (TCM) and Ayurveda. Decoction is well-suited to the extraction of polar compounds, but may have disadvantages for heat-sensitive compounds (100 °C) (Bimakr et al., 2011). Boiling water extraction also has the advantage of denaturing the enzymes capable of hydrolysing heterosides (Bourquelot & Herissey, 1902). Ultrasonic Assisted Extraction (UAE) is recognised as an environmentally friendly extraction technology because solvent volumes are low and extraction times and energy consumption are reduced (Shen et al., 2023).

Results on extraction yields (%) are reported in Tables S1 and S2 (Supplementary Materials). Except for the extraction by hydroalcoholic (60 %) maceration, the best yields were obtained with dried leaves. Fresh and dried leaves differ in their suitability for extraction due to water content. Fresh leaves contain water, which can hinder extraction with certain solvents and may promote microbial growth. Drying reduces water content, improving long-term stability and facilitating extraction with several solvents. Drying is one of the most common plant material preservation procedures because water is necessary for the activity of microorganisms and plant enzymes.

Analysing the extraction procedures, except for D3 extract (decoction of *C. mas* dried leaves), the hydroalcoholic (60 %) maceration resulted as the more efficient technique.

Several solvents, such as water, methanol, ethanol, acetone, and *n*-hexane, have been used to extract bioactive molecules from plants. Out of these solvents, ethanol and ethanol-water mixture (hydroalcoholic solution) provides benefits as they are comparatively more suitable for human consumption in terms of safety. The hydroalcoholic solution for the extraction of polar secondary metabolites is more polar than absolute ethanol. Indeed, it is expected to have a positive influence on the extraction results, especially regarding the phenolic content (Waszkowiak & Gliszczynska-Swigło, 2016).

The total content of phenols, flavonoids, and iridoids (TPC, TFC, and TIC, respectively) of *C. sanguinea* and *C. mas* extracts has been evaluated Tables S3 and S4). The total iridoids content (TIC) ranged from 96.7 to 130.1 mg AU equivalent/g extract for fresh leaves, and from 113.3 to

174.0 mg AU equivalent/g extract for dried leaves. The highest TIC was obtained by ethanol ultrasound-assisted extraction with values of 174.0 and 130.1 mg AU/g for dried and fresh leaves, respectively.

The highest TPC of *C. sanguinea* extracts was obtained by ethanolic maceration of fresh leaves (A1, 355.8 mg CAE/g extract) and decoction of dried leaves (A3; 321.2 mg CA equivalents/g extract). By contrast, the use of ultrasounds-assisted extraction has produced extracts rich in flavonoids for both fresh (A4 sample, 174.5 mg QE equivalents/g extract) and dried leaves (B4 sample, 171.1 mg QE equivalents/g extract). The extract B4 showed the highest iridoids content with a value of 182.7 mg AU equivalents/g extract. To the best of our knowledge, this is the first report that reports the total iridoids content of *C. sanguinea* extracts.

The TPC of *C. mas* extracts ranged from 233.0 to 479.6 mg CA equivalents/g extract for fresh leaves, and from 263.7 to 410.7 mg CA equivalents/g extract for dried leaves, with the highest TPC being for sample C1 and D3. The extracts with the lowest TPC were obtained by UAE of both fresh and dried leaves. TFC ranged from 92.6 to 247.6 mg QE equivalent/g extract for fresh leaves, and from 75.7 to 296.1 mg QE equivalent/g extract for dried leaves. The highest TFC was obtained by decoction.

Our results are in agreement with these reported by Celep et al. (2013) that assessed TPC and TFC of the hydroalcoholic maceration of dried leaves of cornelian cherry. Stanković and Topuzović (2012) extracted the *C. sanguinea* leaves from Serbia with water, methanol, acetone, ethyl acetate and petroleum ether and examined TPC and TFC. The high content of phenols is measured in methanol extract, followed by water extract. Analysing the concentration of total soluble phenolic compounds in all leaf extracts it is noticed that the highest concentration of phenolic compounds are in the extracts obtained using solvents of high polarity. Instead, the highest contents of flavonoids are found in ethyl acetate and acetone extracts.

The analyses by LC-ESI-QTOF-MS allowed the identification of phenolic acids, iridoids and flavonoids as main classes of *Cornus* extracts constituents (Table 1 and Table 2) (Badalica-Petrescu et al., 2014; Bhattachartya et al., 2013; Cai et al., 2013; Cook, 2019; Deng et al., 2013; Drkenda et al., 2014; Guendouze-Bouchefa et al., 2015; Guzhva, 2008; Hatano et al., 1989; Hobbs et al., 2015; Iannuzzi et al., 2021; Korulkina et al., 2004; Krivoruchko, 2014; Lee et al., 2000; Lee et al., 2011; Lee et al., 2021; Li et al., 2014; Malhotra & Misra, 1981; Pawlowska et al., 2010; Popović et al., 2017; Sochor et al., 2014; Tanaka et al., 2001; Yan et al., 2002).

In detail, eight phenolic acids, fourteen flavonoids, three iridoids, one coumarin, one tannin, and (3,4-dihydroxyphenyl)-ethyl-*O*-glucoside were detected in *C. sanguinea* extracts while eight phenolic acids, fourteen flavonoids, six iridoids, and one tannin were identified in *C. mas* extracts. Chromatograms of two selected extracts, such as *C. sanguinea* fresh leaves ethanol maceration (A1) and *C. mas* dried leaves hydroalcoholic maceration (D2), respectively, are reported in Fig. S1 and S2 (Supplementary Materials).

The chemical analysis of *C. sanguinea* extracts led to the identification of quercetin derivatives (galactoside and glucoside) in all *Cornus* samples. Except for decoction (extracts A3 and B3) rutin and kaempferol derivatives (kaempferol 3-*O*-galactoside and kaempferol 3-*O*-glucoside) have been identified in all *C. sanguinea* extracts. Kaempferol 3-*O*-glucuronide was found in all extracts except for both hydroalcoholic extracts A2 and B2, while kaempferol 3-*O*-rutinoside was found in A4 and B1. Isorhamnetin glucuronide and quercetin were identified only in ethanol maceration and ultrasound extracts of fresh leaves (A1 and A4). Myricitrin and quercetin 3-*O*-xyloside were detected in ethanol maceration, ultrasound extracts of fresh leaves (A1 and A4) and decoction of dried leaves (B3); in addition, myricitrin was also found in fresh leaves decoction (A3) and hydroalcoholic maceration of dried leaves (B2). Myricetin 3-*O*-arabinoside was revealed in ethanol maceration and ultrasound extracts of fresh leaves (A1 and A4) and both leaves extracts obtained by hydroalcoholic maceration (A2 and B2). In ethanol ultrasound extract of fresh leaves and ethanol maceration of dried leaves (A4 and B1) kaempferol 3-*O*-rutinoside was identified. Myricetin galloylarabinoside and quercetin acetylglycoside were specifically identified in fresh leaves obtained by ethanol and hydroalcoholic maceration (A1 and A2). Chlorogenic acid and ellagic acid characterized all *C. sanguinea* extracts. Gallic acid was found also in all extracts except for the ultrasound-assisted extracts A4 and B4. Syringic acid, phenylacetic acid and 2-galloyl-4-caffeoyl threonic acid were identified in ethanol maceration of fresh leaves (A1), and hydroalcoholic maceration of dried leaves (B2). 2-Galloyl-4-caffeoyl threonic acid was detected also in the ultrasound-assisted extract of fresh leaves (A4). Neochlorogenic acid and quinic acid was detected only in the extract obtained by ethanol maceration of fresh leaves (A1). Scopolin was described in extracts obtained by ethanol maceration of fresh and dried leaves (A1 and B1), and ultrasound-assisted extraction of fresh leaves (A4). A β-(3,4-dihydroxyphenyl)-ethyl-*O*-glucoside was previous detected in *C. sanguinea* fruits (Lee et al., 2021); herein, this compound was found in ultrasound extract obtained by fresh leaves (A4) and ethanol maceration of dried leaves (B1). The tannin gemin D was identified in the extract obtained by ethanol maceration of fresh leaves (A1). Iridoids detected in *C. sanguinea* extracts were cornuside, sweroside and verbenalin.

The phytochemical analysis of the *C. mas* extracts revealed the presence of kaempferol (galactoside, glucoside and glucuronide) derivatives, quercetin (galactoside, glucoside, glucuronide, rhamnoside, and xyloside) derivatives, and quercetin 3-*O*-glucuronide-6″-methyl ester. Rutin and quercetin 3-*O*-galactosyl 7-*O*-rhamnoside were identified in the extracts obtained by ultrasound-assisted extraction of fresh leaves (C4), hydroalcoholic maceration of dried leaves (D2) and ethanol maceration of both fresh and dried leaves (C1 and D1).

Kaempferol 3-*O*-rutinoside was found in the ethanol maceration and ultrasound-assisted extraction of fresh leaves and in dried extracts obtained by hydroalcoholic maceration. Quercetin was detected only in the extracts obtained by hydroalcoholic maceration of fresh and dried leaves (C2 and D2). Six iridoids, namely cornuside, loganic acid, sweroside, secologanin, verbenalin and α-dihydrocornic acid, were found in *C. mas* extracts. Secologanin, sweroside, and cornuside characterized all *C. mas* leaf extracts while loganic acid was identified in all extracts except for hydroalcoholic maceration of dry matrix (D2). Verbenalin was found only in the extracts obtained by ultrasound-assisted extraction of fresh matrix (C4) and dried leaves extracts obtained by ethanol maceration (D1). α-Dihydrocornic acid was herein described for the first time in *C. mas*. This iridoid was previously identified only in *C. capitata* (Tanaka et al., 2001). Analysing phenolic acids, ellagic acid 4-*O*-rutinoside, ferulic acid, and gallic acid are present in all *C. mas* extracts, while gallic acid 4-*O*-glucoside was detected only in extracts obtained by ethanol maceration (C1) and ultrasound-assisted extraction (C4) of fresh leaves.

Ethyl caffeate was identified in the ethanol maceration of both *C. mas* fresh and dried leaves (C1 and D1) while chlorogenic acid was found only in the hydroalcoholic maceration C2 and D2. Ellagic acid and quinic acid were identified in the hydroalcoholic maceration of dried leaves (D2). The tannin gemin D was identified in all *C. mas* extracts.

Most of the identified compounds were previously described in the *Cornus* genus, except for myricetin derivatives, ellagic acid 4-*O*-rutinoside, and ethyl caffeate. The mass spectra and fragmentations observed, as well as the UV spectra of the latter, provide concordant clues that have made it possible to establish their identification.

The A1 and D2 extracts, which demonstrated strong hypoglycaemic activity – mainly through α-glucosidase inhibition - as well as notable radical scavenging effects and lipid peroxidation inhibitory activity, were subjected to fractionation using Amberlite XAD-16 resin. This apolar resin offers better adsorption and desorption of polyphenols compared to a polar resin (Seif Zadeh & Zeppa, 2022). Three fractions, the first eluted with water, the second and third attained with 80 % and absolute ethanol, have been obtained and chemically analysed. Generally, the fractions eluted with water showed all those compounds not absorbed by the resin while the second fractions are mainly composed of

Table 1
LC-ESI-QTOF-MS analyses of blood twig dogwood (*C. sanguinea*) leaves extracts.

Compounds	Rt (min)	MH^+	Error (ppm)	Score (%)	MS fragment (*m/z*)	UV λ (nm)[#]	A1	A2	A3	A4	B1	B2	B3	B4	Reference
Phenolic acids															
Chlorogenic acid°	9.8	355.1029	1.6	100		242, 325	+	+	+	+	+	+	+	+	Deng et al., 2013
Ellagic acid °	12.8	303.0140	1.2	100		255, 365	+	+	+	+	+	+	+	+	Deng et al., 2013
Gallic acid°	3.2	171.0287	1.1	100		217, 271	+	+	+		+	+	+		Deng et al., 2013
2-Galloyl-4-caffeoyl-threonic acid (*)	12.1	451.0876	1.3	99		255, 294, 330	+			+		+			Lee et al., 2000
Neochlorogenic acid	6.7	355.1029	1.1	100		245, 325	+								Popović et al., 2017
Phenylacetic acid	2.1	137.0602	2.1	97		205, 259	+		+			+	+		Cook, 2019
Quinic acid°	0.9	193.0706	0.9	100		212	+								Drkenda et al., 2014
Syringic acid°	10.6	199.0606	2.3	89		218, 273	+					+			Guendouze-Bouchefa et al., 2015
Flavonoids															
Isorhamnetin glucuronide	14.0	493.0982	2.2	97	316.2670	215, 256, 354	+			+					Li et al., 2014
Kaempferol 3-*O*-galactoside (**)	13.2	449.1077	1.5	100	287.2278	210, 263, 344	+	+		+	+	+		+	Pawlowska et al., 2010
Kaempferol 3-*O*-glucoside (**)	13.2	449.1077	1.5	100	287.2287	210, 265, 346	+	+		+	+	+		+	Pawlowska et al., 2010
Kaempferol 3-*O*-glucuronide	13.7	463.0876	1.1	100	287.2283	210, 264, 345	+		+	+	+		+	+	Badalica-Petrescu et al., 2014
Kaempferol 3-O-rutinoside	12.9	595.1663	2.2	81	287.2279	210, 265, 342				+	+				Li et al., 2014
Myricetin 3-*O*-arabinoside (*)	12.6	451.0876	0.8	100	318.0434	219, 253, 365	+	+		+		+			Yan et al., 2002
Myricetin galloylarabinoside	13.8	603.0986	1.5	98	318.0440	212, 265, 366	+	+							Korulkina et al., 2004
Myricitrin	10.9	467.0825	0.8	100	318.0433	212, 257, 360	+		+	+		+	+		Hobbs et al., 2015
Quercetin°	16.8	303.0504	1.2	100		213, 255, 353	+			+					Sochor et al., 2014
Quercetin acetylglycoside	13.9	507.1138	1.1	100	303.0489	213, 252, 354	+	+							Bhattachartya et al., 2013
Quercetin 3-*O*-galactoside (Hyperoside) °(***)	12.8	465.1031	1.7	100	303.0497	217, 278, 350	+	+	+	+	+	+	+	+	Popović et al., 2017
Quercetin 3-*O*-glucoside (Isoquercitrin) °(***)	12.8	465.1031	1.7	100	303.0499	215, 253, 353	+	+	+	+	+	+	+	+	Popović et al., 2017
Quercetin 3-*O*-xyloside	13.5	435.7749	0.6	100	303.0488	212, 254, 356	+			+			+		Pawlowska et al., 2010
Rutin°	12.4	611.1612	1.3	88	303.0486	213, 253, 352	+	+		+	+	+		+	Popović et al., 2017
Coumarin															
Scopolin	9.1	355.1029	1.6	96		300, 345	+			+	+				Guzhva, 2008
Iridoids															
Cornuside°	12.0	543.1713	0.5	100		218, 273	+	+		+		+			Deng et al., 2013
Sweroside°	10.0	359.1355	6.1	98	197.0795	245	+	+		+					Deng et al., 2013
Verbenalin	9.5	389.1446	0.4	100	227.1630	238	+	+		+					Cai et al., 2013
Tannin															
Gemin D	8.8	635.0884	1.1	100		221, 265	+								Hatano et al., 1989

(*continued on next page*)

Table 1 (*continued*)

Compounds	Rt (min)	MH^+	Error (ppm)	Score (%)	MS fragment (*m/z*)	UV λ (nm)#	A1	A2	A3	A4	B1	B2	B3	B4	Reference
Other compounds															
(3,4-dihydroxyphenyl)-ethyl-*O*-glucoside	1.5	317.1236	0.9	100	137.0603	215, 314				+	+				Iannuzzi et al., 2021

A: *C. sanguinea* fresh leaves, B: *C. sanguinea* dried leaves; 1. Ethanol maceration; 2. Hydroalcoholic (60 %) maceration; 3. Decoction; 4. Ethanol ultrasound assisted extraction. ° Identified with standard compound. (*)(**) (***) interchangeable 2 peaks. # detected by DAD spectrophotometer.

iridoids and flavonoids. The third fractions contain only flavonoids.

LC-MS analyses (Table 3) of *C. sanguinea* fractions revealed the presence in A1a of gallic acid and 1-*O*-galloyl-*D*-sedoheptulose and some unknown compounds (Badalica-Petrescu et al., 2014; Deng et al., 2013; Lee et al., 1989; Lee et al., 2000; Lee et al., 2008; Pawlowska et al., 2010; Popović et al., 2017; Sochor et al., 2014). The seco-iridoid cornuside and the putative lignan cornuskoside A, different flavonoids (kaempferol derivatives, quercetin, and quercetin derivatives) and some unknown compounds were found in A1b. Fraction A1c showed the presence of quercetin, quercetin 3-*O*-xyloside, isoquercitrin and some unknown compounds.

In D2a gallic acid and traces of ellagic acid were found (Table 4) (Badalica-Petrescu et al., 2014; Deng et al., 2013; Hatano et al., 1989; Li et al., 2014; Malhotra & Misra, 1981; Pawlowska et al., 2010; Sochor et al., 2014). D2b is characterized by the presence of three iridoids namely cornuside, sweroside, and secologanin, one phenolic acid such as ellagic acid with its derivative, ellagic acid 4-*O*-rutinoside, and several flavonoids. D2c showed kaempferol derivatives, quercetin, quercetin derivatives, and ellagic acid as main constituents.

The chemical analysis of fractions obtained using the XAD-16 amberlite resin (A1a-A1c and D2a-D2c) revealed the presence of unidentified compounds in the crude extracts, such as 1-*O*-galloyl-D-sedoheptulose, digalloylglycoside and its isomer, quercetin 3-*O*-glucuronide, cornuskoside A and 4-caffeoyl-2,3-digalloyl-threonic acid. After treatment with this resin, which is selective for phenolic groups, these compounds are retained and can be detected after elution. All these compounds were identified in other *Cornus* species as reported in literature (Lee et al., 2000, 1989, 2008; Popović et al., 2017), but for the first time in *C. sanguinea* leaves.

3.2. Hypoglycaemic properties and molecular docking studies

The enzymes α-amylase and α-glucosidase are widely exploited as targets to counteract post-prandial hyperglycaemia in type 2 diabetes. Herein, we applied in vitro methods to provide insights into the α-amylase and α-glucosidase inhibitory potential of *C. mas* and *C. sanguinea* extracts and fractions, and the pure compounds sweroside, cornuside, and ellagic acid.

Results (IC_{50} values) are reported in Table 5. Overall, a higher activity towards α-glucosidase compared to α-amylase can be observed. The ethanol extract of fresh *C. sanguinea* leaves (sample A1) demonstrated the strongest α-glucosidase inhibitory activity, with an IC_{50} value of 9.8 μg/mL. Against α-amylase the most active extract is A2 (hydroalcoholic maceration) of fresh leaves with an IC_{50} value of 174.0 μg/mL.

Among the *C. mas* extracts, D1 and D2 demonstrated the highest activity against α-glucosidase, with IC_{50} values of 32.2 and 16.6 μg/mL, respectively. In contrast, C1, A2, and A4 extracts showed the most potent inhibition of α-amylase, with IC_{50} values of 142.5, 174.0, and 189.8 μg/mL, respectively. The fractionation by XAD-16 resin of both extracts A1 (ethanol maceration of *C. sanguinea* fresh leaves) and D2 (hydroalcoholic maceration of *C. mas* dried leaves) did not result in an enhancement of hypoglycemic activity, suggesting a synergistic action of the components of the phytocomplex.

Remarkable results were obtained by testing the three pure compounds. Sweroside was the most active with IC_{50} values of 0.9 and 2.4 μg/mL against α-glucosidase and α-amylase, respectively. Cornuside and ellagic acid strongly inhibited α-glucosidase with IC_{50} values of 5.8 and 2.7 μg/mL, respectively. Given the availability on the Protein Data Bank of several crystallographic structures for the two enzymes investigated in this study, the structures with PDB codes 3TOP for α-glucosidase and 4 W93 for α-amylase were selected for molecular docking studies. Specifically, 3TOP corresponds to the carboxy-terminal active domain (CtMGAM) of α-glucosidase, and, in this structure, the protein is complexed with the known inhibitor α-acarbose (AC1), while in 4 W93, pancreatic α-amylase is complex with its known inhibitor montbretin A (3 L9), an acylated flavonol glycoside (Ren et al., 2011; Williams et al., 2015). These experiments sought to verify whether the biological activity of the *Cornus* extract observed in our biological assays could be ascribed to a direct interaction of its main components and the two target proteins. Accordingly, cornuside, ellagic acid, and sweroside were docked with the 3TOP protein, and their binding modes were compared to the crystallographic ligand, following a procedure already adopted in previous studies (De Luca et al., 2022; Grande et al., 2021). The resulting binding energy values for the three compounds (−8.9, −8.2, and − 8.2 kcal/mol for cornuside, ellagic acid, and sweroside, respectively) were slightly more favourable than that of acarbose, previously calculated in a re-docking experiment (−7.92 kcal/mol) (Tundis et al., 2023).

As shown in Fig. 1 (panels A-E), the compounds occupy the same region within the binding site, surrounded by the protein residues Tyr1251, Gln1372, Trp1355, Lys1460, Arg1510, Asp1526, and Phe1559. In particular, cornuside fits into this region by establishing hydrogen bonds with the Tyr1251, Gln1372, and Arg1377 protein residues through the hydroxyl groups of the tetrahydropyran ring, with Arg1510 via the hydroxyl groups of the triol, and with Thr1586 through the carbonyl oxygen of the central dihydropyran nucleus.

Ellagic acid interacts with the binding site by hydrogen bonds between the OH groups of its tetracyclic chromeno[5,4,3-*cde*]chromene-5,10-dione core and the Asp1157, Trp1369, Arg1510, and Asp1526 residues. Meanwhile, sweroside establishes hydrogen bonds with Lys1460 and Asp1526 through the hydroxyl groups of the tetrahydropyran ring. In all three cases, several hydrophobic interactions further contribute to stabilizing the complexes (Table 6). These results suggest that the molecules may bind more readily to glucosidase than acarbose.

This observation is further corroborated by the calculated inhibition constant (Ki) values (1.01, 2.7, and 26.6 μM for cornuside, ellagic acid, and sweroside, respectively). As is well known, the lower the Ki value, the more strongly the inhibitor binds to the target enzyme, reinforcing the hypothesis that these molecules can effectively bind with high affinity to α-glucosidase. Additionally, the calculated ligand efficiency (LE) values, ranging from 0.35 to 0.36 kcal/mol, highlight the favourable binding contribution likely resulting from efficient molecular interactions that are not solely dependent on molecular size.

The same protocol has been applied to investigate the binding mode of the three phytochemicals to α-amylase, using 4 W93. The crystallographic ligand of this structure is montbretin A, a known plant metabolite proposed as an antidiabetic and anti-obesity remedy due to its potent and specific inhibition of the human pancreatic α-amylase. The core structure of montbretin A consists of a myricetin unit linked to a caffeic acid moiety through a disaccharide, with the myricetin core

Table 2
LC-ESI-QTOF-MS analyses of Cornelian cherry (*C. mas*) leaves extracts.

Compound	Rt (min)	MH^+/ MNa^+	Error (ppm)	Score (%)	MS fragment (*m/z*)	UV λ[#] (nm)	C1	C2	C3	C4	D1	D2	D3	D4	Reference
Phenols															
Chlorogenic acid°	9.8	355.1029	1.6	100		242, 325		+				+			Deng et al., 2013
Ellagic acid°	12.8	303.0140	0.9	100		255, 365						+			Deng et al., 2013
Ellagic acid 4-*O*-rutinoside	12.3	611.1248	1.2	100	303.0136	274	+	+	+	+	+	+	+	+	Malhotra & Misra, 1981
Ethyl caffeate	11.0	209.0813	2.1	88		298, 322	+				+				Lee et al., 2021
Ferulic acid°	1.7	195.0652	0.9	100		325	+	+	+	+	+	+	+	+	Krivoruchko, 2014
Gallic acid°	3.2	171.0287	1.1	100		217, 271	+	+	+	+	+	+	+	+	Deng et al., 2013
Gallic acid 4-*O*-glucoside	3.1	355.0641	1.5	99	171.0257	256, 298	+			+					Lee et al., 2011
Quinic acid°	0.9	193.0706	0.9	100		212						+			Drkenda et al., 2014
Flavonoids															
Kaempferol 3-*O*-galactoside (**)	13.2	449.1077	1.5	100	287.2257	210, 263, 344	+	+	+	+	+	+	+	+	Pawlowska et al., 2010
Kaempferol 3-*O*-glucoside (**)	13.2	449.1077	1.5	100	287.2300	210, 265, 346	+	+	+	+	+	+	+	+	Pawlowska et al., 2010
Kaempferol 3-*O*-glucuronide	13.7	463.0876	1.1	100	287.2278	210, 264, 345	+	+	+	+	+	+	+	+	Badalica-Petrescu et al., 2014
Kaempferol 3-*O*-rutinoside	12.9	595.1663	1.2	98	287.2287	210, 265, 342	+			+		+			Li et al., 2014
Quercetin°	16.8	303.0504	1.2	100		213, 255, 353		+				+			Sochor et al., 2014
Quercetin 3-*O*-galactoside (Hyperoside) °(*)	12.8	465.1031	1.5	100	303.0499	217, 278, 350	+	+	+	+	+	+	+	+	Pawlowska et al., 2010
Quercetin 3-*O*-galactosyl 7-*O*-rhamnoside (****)	12.4	611.1612	1.3	100	303.0479	212, 253, 356	+			+	+				Badalica-Petrescu et al., 2014
Quercetin 3-*O*-glucoside (Isoquercitrin) °(*)	12.8	465.1031	1.5	100	303.0493	215, 253, 353	+	+	+	+	+	+	+	+	Pawlowska et al., 2010
Quercetin 3-*O*-glucoronide isomer (***)	12.3	479.0825	1.1	100	303.0476	215, 247, 354						+	+	+	Pawlowska et al., 2010
Quercetin 3-*O*-glucuronide (***)	13.0	479.0825	1.8	100	303.0475	216, 244, 354	+	+	+	+	+	+	+	+	Pawlowska et al., 2010
Quercetin 3-*O*-glucuronide-6″-methyl ester	13.1	493.0982	1.5	97	303.0479	215, 247, 354	+	+	+	+	+	+	+	+	Pawlowska et al., 2010
Quercetin 3-*O*-xyloside	13.5	435.7749	0.6	100	303.0483	212, 254, 356	+	+	+	+	+	+	+	+	Pawlowska et al., 2010
Quercitrin	13.6	449.1079	1.5	100	303.0487	213, 254, 356	+	+	+	+	+	+	+	+	Pawlowska et al., 2010
Rutin° (****)	12.4	611.1612	0.7	100	303.0488	213, 253, 352	+			+	+	+			Pawlowska et al., 2010
Iridoids															
α-Dihydrocornic acid	6.3	377.1447	0.9	100		215	+		+	+	+	+	+	+	Tanaka et al., 2001
Cornuside°	12.0	543.1713	0.2	100		218, 273	+	+	+	+	+	+	+	+	Deng et al., 2013
Loganic acid	6.4	377.1447	1.1	100		238	+	+	+	+	+		+	+	Deng et al., 2013
Verbenalin	9.5	389.1446	0.5	100	227.0917	238				+	+				Hatano et al., 1989
Secologanin	9.0	389.1447	1.1	100		245	+	+	+	+	+	+	+	+	Deng et al., 2013
Sweroside°	8.0	359.1342	1.2	100		245	+	+	+	+	+	+	+	+	Deng et al., 2013
Tannin															
Gemin D	8.8	635.0884	1.1	100		221, 265	+	+	+	+	+	+	+	+	Hatano et al., 1989

C: *C. mas* fresh leaves; D: *C. mas* dried leaves. 1. Ethanol maceration; 2. Hydroalcoholic (60 %) maceration; 3. Decoction; 4. Ethanol ultrasound assisted extraction. ° Identified with standard compounds; (*)(**) (***)(****) interchangeable or 2 peaks. # detected by DAD spectrophotometer.

Table 3
LC-MS analyses of *C. sanguinea* fractions obtained by amberlite XAD-16 resin.

Compound	Rt (min)	MM	UV λ (nm)	A1a	A1b	A1c	Reference
Unknown	1.4	294	200	+			
Unknown	1.9	308	200	+			
Gallic acid	3.7	170	216, 270	+			Deng et al., 2013
1-*O*-galloyl-*D*-sedoheptulose	4.7	362	216, 275	+			Lee et al., 1989
Unknown	8.9	184	216, 275		+	+	
Digalloylglycoside (*)	9.9	484	216, 275		+		Lee et al., 1989
Quercetin 3-*O*-xyloside	13	434	202, 250, 344		+	+	Pawlowska et al., 2010
Digalloylglycoside isomer (*)	13.7	484	216, 275		+		Lee et al., 1989
Cornuside	21	542	220, 277		+		Deng et al., 2013
2-galloyl-4-caffeoyl-threonic acid (**)	21.5	450	217, 250, 329		+		Lee et al., 2000
2-galloyl-4-caffeoyl-threonic acid isomer (**)	21.7	450	217, 250, 329		+		Lee et al., 2000
Hyperoside(***)	23.4	464	217, 278, 350		+		Popović et al., 2017
Isoquercitrin(***)	23.7	464	219, 278, 350		+		Popović et al., 2017
Quercitrin or Kaempferol 3-*O*-glucoside or Kaempferol 3-*O*-galactoside	24.3	448	217, 278, 350		+		Popović et al., 2017; Pawlowska et al., 2010
Quercetin 3-*O*-glucuronide	24.7	478	205, 258, 356		+		Popović et al., 2017
Cornuskoside A	24.9	492	243, 282		+		Lee et al., 2008
Kaempferol 3-*O*-glucuronide	25.2	462	210, 267, 340		+		Badalica-Petrescu et al., 2014
4-Caffeoyl-2,3-digalloyl-threonic acid	25.6	602	218, 285, 330		+		Lee et al., 2000
Quercetin	27.7	302	203, 257, 375		+	+	Sochor et al., 2014

A1: ethanol maceration of *C. sanguinea* fresh leaves; a: fraction H_2O; b: fraction 80 % EtOH; c: fraction absolute EtOH. (*)(**)(***) interchangeable peaks or isomer.

functionalised by two carbohydrates chains-one attached at the O3 position of the benzopyrone ring and the other at the C4 position of the phenyl group-and a caffeic acid unit connected to the C6 of the first glucose in the chain.

Crystallographic studies on the montbretin A-human α-amylase complex highlighted the critical importance of this core structure. These findings uncovered a distinctive inhibition mechanism in which intramolecular π-stacking interactions between the myricetin and caffeic acid moieties arrange the hydroxyl groups on their rings, facilitating hydrogen bonding with the α-amylase catalytic residues, Asp197 and Glu233 (Williams et al., 2015).

The structure of α-amylase consists of three distinct domains, with its active site placed at one end of a triosephosphate isomerase barrel. In our docking studies, cornuside, ellagic acid, and sweroside fit seamlessly into this binding site, interacting with residues essential for catalysis and mimicking the binding mode of the crystallographic ligand, despite being smaller in size than this latter (Fig. 2).

Specifically, cornuside interacts with the binding pocket by forming hydrogen bonds with Asp197, Ala198, Ser199, Glu233, and Ile235 residues through the hydroxyl groups of the benzotriol, while the hydroxyl group in the *meta*-position of the tetrahydropyran moiety establishes a further hydrogen bond with Asp197.

Ellagic acid interacts by hydrogen bonds with Asp197, Ala198, and Lys200 via its pyrocatechol structure, as well as with Ile235 through its tetracyclic chromenochromendione core. Sweroside also establishes hydrogen bonds with Arg195, Asp197, and Ala198 through hydroxyl groups of the tetrahydropyran ring. Several hydrophobic interactions further enhance the stability of these complexes (Table 6).

The calculated binding energies for the three molecules were slightly less favourable than that of the crystallographic ligand, with values of −7.3, −7.9, and − 6.9 kcal/mol for cornuside, ellagic acid, and sweroside, respectively, compared to the crystallographic ligand's value of −8.05 kcal/mol, as determined in a previous re-docking study (Tundis et al., 2023).

This is further supported by the calculated inhibition constant (K*i*) values, which indicate that ellagic acid exhibits the most favourable binding affinity to α-amylase (K*i* = 2.7 μM), outperforming both cornuside (7.2 μM) and sweroside (13.7 μM).

Moreover, the ligand efficiency (LE) values, ranging from 0.30 to 0.38 kcal/mol per heavy atom, reflect an efficient binding interaction, with sweroside showing the highest LE despite its weaker binding affinity. These results highlight that all three compounds interact efficiently with the enzyme active site, achieving a favourable balance between molecular size and binding strength.

Nevertheless, these findings suggest that these compounds could serve as suitable ligands for the target protein.

To evaluate whether the activity of the extract, found in biological experiments to be higher than that of the isolated components, could be attributed to the simultaneous binding of multiple molecules to the enzyme, a blind docking protocol was performed for both proteins. By systematically exploring the entire protein volume of 3TOP, we identified three primary hot spots where ligands accommodate when the ligand-binding site is occupied, highlighting potential areas for further investigation in drug design.

The most populated site (referred to as site a in panel A, Fig. 3), surrounded by Asp1281, Arg1285, Gln1286, Ser1292, and Ile1587 residues, was selected for a refined docking experiment, during which the binding site was kept occupied by a cornuside moiety. As a result, all three compounds effectively bound to this region, as reflected in their favourable binding energy values (−7.4 kcal/mol for cornuside and ellagic acid, respectively, and − 7.8 kcal/mol for sweroside). These observations are consistent with the inhibition constant values, which further support the binding ability of these compounds to the secondary site of α-glucosidase. In particular, sweroside exhibited the lowest Ki values (3.2 μM), suggesting a stronger predicted affinity than cornuside and ellagic acid (K*i* = 6.0 μM). Moreover, the LE values, ranging from 0.31 to 0.43 kcal/mol, highlight the capacity of these small molecules to interact effectively with the protein, especially sweroside, which shows the highest LE.

The establishment of hydrogen bonds with Asp1281, Arg1285, Gln1286 and Ser1292 as well as a hydrophobic interaction with Ile1587 in this site, shared by all the three phytochemicals, seem crucial in the complexes formation. These findings suggest that the enzyme structure is amenable to allosteric modulation, thereby supporting the possibility of a synergistic interaction among the components of the extract. A detailed analysis of the docking results for the best pose of the molecules is this secondary site is reported in Table 7, while the best docking conformations are depicted in Fig. 3.

Also, in the case of α-amylase, a systematic exploration of the entire protein volume of 4 W93 led to identifying a subsite that accommodates

Table 4
LC-MS analyses of *C. mas* fractions obtained by amberlite XAD-16 resin.

Compound	Rt (min)	MM	UV λ (nm)	D2a	D2b	D2c	Reference
Gallic acid	2.13	170	216, 270	+			Deng et al., 2013
Gemin D	3.20	634	221, 265		+		Hatano et al., 1989
Sweroside	7.20	358	245		+		Deng et al., 2013
Secologanin	7.83	388	245		+		Deng et al., 2013
Kaempferol 3-*O*-rutinoside isomer	15.21	594	210, 265, 342		+	+	Li et al., 2014
Kaempferol 3-*O*-rutinoside isomer	16.71	594	210, 265, 342		+	+	Li et al., 2014
Cornuside	17.58	542	218, 273		+		Deng et al., 2013
Quercetin 3-*O*-xyloside	18.27	434	212, 254, 356		+	+	Pawlowska et al., 2010
Quercitrin	19.05	448	213, 254, 356		+	+	Pawlowska et al., 2010
Ellagic acid	19.50	302	255, 365	+	+	+	Deng et al., 2013
Rutin	19.86	610	213, 253, 352		+	+	Pawlowska et al., 2010
Ellagic acid 4-*O*-rutinoside	20.15	610	258, 314		+		Malhotra & Misra, 1981
Hyperoside(*)	20.42	464	213, 278, 350		+	+	Pawlowska et al., 2010
Isoquercetin (*)	20.65	464	213, 253, 353		+	+	Pawlowska et al., 2010
Kaempferol 3-*O*-glucuronide	21.69	462	210, 268, 350		+	+	Badalica-Petrescu et al., 2014
Quercetin 3-*O*-glucuronide	21.84	478	205, 258, 356		+	+	Pawlowska et al., 2010
Quercetin	26.60	302	203, 257, 375			+	Sochor et al., 2014

D2: hydroalcoholic maceration of *C. mas* dried leaves; a: fraction H_2O; b: fraction 80 % EtOH; c: fraction absolute EtOH. (*) or isomer.

the majority of compound poses when the main active site is occupied, suggesting its potential role as an alternative binding region within the enzyme (site a in panel A, Fig. 4). This secondary site, located in an outer region of the protein, was subsequently selected for a refined docking experiment. As a result, all three compounds, cornuside, ellagic acid, and sweroside, bound to this site, with favourable binding energies values of −7.0, −8.1, and − 7.1 kcal/mol, respectively.

The binding affinities are corroborated by the calculated K*i* values, which again point to ellagic acid as the most promising compound, with a K*i* value of 2.0 μM, significantly lower than those of cornuside (11.8 μM) and sweroside (9.9 μM). At the same time, LE values ranging from 0.30 to 0.40 kcal/mol confirm efficient binding despite the smaller size of these phytochemicals, particularly for sweroside, which maintains a favourable efficiency even with a moderate affinity. In particular, cornuside established several hydrogen bonds due both to the high number of OH groups in its structure as well as to the flexibility of the molecule resulting from 18 rotatable dihedral angles.

The protein residues involved in these interactions include Gly9, Arg10, Thr11, Arg398, Asp402 and Gly403. On the other hand, ellagic acid interacts by hydrogen bond with Ser289 Pro332, Gly3334, and Thr6. This last residue also plays a crucial role in the binding of sweroside to this region. The complexes are stabilised by additional hydrophobic interactions.

Overall, the molecular docking results combined with the evaluation of inhibition constants (K*i*), and ligand efficiency (LE) across both the primary and secondary sites of α-glucosidase and α-amylase confirm the potential of the three phytochemicals as enzyme ligands. Notably, ellagic acid consistently exhibits lower K*i* values and high LE, indicating both strong and efficient binding.

Sweroside, while generally displaying weaker binding energies, often compensates with the highest ligand efficiency. These results provide a molecular basis for the observed biological activity of the Cornus extract and support the hypothesis that synergistic interactions among its components, possibly mediated by allosteric binding sites, may enhance overall inhibitory potential. A more detailed analysis of the docking results for the best pose of the ligand molecules in site a is reported in Table 7, while the best docking conformations are depicted in Fig. 4. These results indicate that this secondary site may function as an allosteric site, justifying the greater activity of the mixture of the active compounds in the *Cornus* leaves extracts when compared to that of the individual molecules, thereby suggesting a synergistic effect.

3.3. *In silico prediction of ADMET properties*

The ADMET (Absorption, Distribution, Metabolism, Excretion, and Toxicity) profiles of the selected compounds were evaluated using SwissADME (http://www.swissadme.ch/), revealing promising pharmacokinetic and drug-likeness features supporting their potential as therapeutic agents (Lotfi et al., 2025). A key aspect of the evaluation involved Lipinski's Rule of Five, a widely accepted guideline in drug discovery to estimate the oral bioavailability of small molecules (Lipinski, 2004). According to this rule, drug-like compounds generally have a molecular weight $\leq$ 500 Da, a LogP $\leq$5, no more than 5 hydrogen bond donors, and no more than 10 hydrogen bond acceptors ensuring an appropriate balance between hydrophilicity and lipophilicity necessary for effective absorption and distribution.

Furthermore, lipophilicity was assessed using the consensus LogP, calculated as the mean of five independent LogPo/w predictions (iLOGP, XLOGP3, WLOGP, MLOGP, and SILICOS-IT). Additional pharmacokinetic properties including gastrointestinal (GI) absorption, blood–brain barrier (BBB) permeability, and skin permeation (LogKp, cm/s), and bioavailability scores, were also estimated (Table 8; Fig. S3-S6, Supplementary Materials). In particular, cornuside displayed high polarity and low lipophilicity (consensus LogPo/w = −0.35). However, it exhibited low GI absorption, was not BBB permeable, and presented a low skin permeation rate (LogKp = −9.76). The bioavailability score was low (0.11), and it violated three of Lipinski's rules, and other drug-likeness criteria, indicating poor membrane permeability and limited oral bioavailability, consistent with its structural complexity and high polarity.

However, these findings are consistent with existing literature, which indicates that the sugar moiety in glycosylated compounds mainly affects pharmacokinetics but is not essential for interaction with the molecular target. Indeed, glycosides are known to undergo enzymatic hydrolysis by colonic microflora β-glucosidases, a process considered the rate-limiting step for the release and absorption of the active aglycone (Grande et al., 2021; Guo et al., 2020).

In view of these considerations, we opted to investigate also the drug-like characteristics of the aglycone form. As expected, cornuside aglycone displays significantly improved drug-like properties. The absence of the sugar moiety results in full compliance with Lipinski's criteria, a more balanced lipophilicity profile (consensus LogP = 1.15), and showed favourable GI absorption and BBB permeability, indicating an enhanced oral bioavailability while preserving the structural features responsible for biological activity.

Ellagic acid demonstrates reasonable drug-likeness. In fact, it showed a good solubility, a high bioavailability score (0.55), and fulfilled most drug-likeness criteria with only one violation each in Lipinski and Ghose

Table 5
Biological properties of *Cornus* extracts, fractions, and pure compounds.

Sample	α-Glucosidase Inhibition (IC_{50} μg/mL)	α-Amylase Inhibition (IC_{50} μg/mL)	NO production Inhibition (IC_{50} μg/mL) HFF-1 cells	NO production Inhibition (IC_{50} μg/mL) RAW 264.7 cells	β-Carotene bleaching test (IC_{50} μg/mL)		FRAP test (μM Fe(II)/g)	ABTS test (IC_{50} μg/mL)
					t = 30 min	*t = 60* min		
A1	9.8 ± 0.5****	568.2 ± 5.6****	38.0 ± 1.1****	29.2 ± 0.8****	10.5 ± 0.9****	9.2 ± 0.8****	92.8 ± 2.5****	0.4 ± 0.03
A2	341.3 ± 2.7****	174.0 ± 1.8****	38.9 ± 1.9****	30.6 ± 2.3****	NA	11.4 ± 0.9****	98.9 ± 3.0****	1.2 ± 0.02
A3	182.8 ± 1.9****	449.1 ± 4.5****	34.3 ± 2.5****	26.0 ± 3.4****	12.4 ± 0.5****	44.1 ± 2.3****	97.5 ± 3.0****	0.4 ± 0.01
A4	554.2 ± 4.6****	904.5 ± 6.3****	41.5 ± 1.8****	32.7 ± 0.6****	12.0 ± 0.8****	11.3 ± 0.5****	94.1 ± 2.8****	1.1 ± 0.07
B1	63.4 ± 1.2****	682.0 ± 3.8****	38.3 ± 1.7****	26.2 ± 1.5****	12.2 ± 0.7****	11.2 ± 0.4****	101.4 ± 4.1****	0.8 ± 0.01
B2	137.3 ± 3.6****	446.4 ± 3.5****	44.3 ± 2.0****	36.4 ± 2.4****	10.7 ± 1.0****	9.1 ± 0.1****	101.2 ± 4.8****	1.2 ± 0.02
B3	142.5 ± 2.5****	277.4 ± 2.4****	39.3 ± 1.1****	28.0 ± 0.9****	14.3 ± 1.0****	NA	100.7 ± 4.7****	1.0 ± 0.01
B4	227.5 ± 2.7****	444.7 ± 4.6****	34.8 ± 0.8****	22.3 ± 1.2****	13.2 ± 0.9****	12.7 ± 1.0****	96.8 ± 4.0****	0.8 ± 0.08
C1	192.4 ± 8.2****	142.5 ± 2.0****	21.3 ± 1.4****	19.6 ± 1.1****	86.3 ± 2.8****	73.5 ± 2.2****	18.0 ± 2.2****	1.2 ± 0.1
C2	162.7 ± 8.0****	348.3 ± 3.6****	26.8 ± 2.3****	24.1 ± 1.9****	75.3 ± 2.6****	68.5 ± 2.3****	18.2 ± 1.7****	1.1 ± 0.5
C3	189.8 ± 7.1****	244.1 ± 2.4****	34.9 ± 2.5****	30.3 ± 2.1****	13.9 ± 1.0**	11.5 ± 1.6	16.5 ± 2.8****	1.1 ± 0.4
C4	362.4 ± 4.6****	189.8 ± 2.3****	42.1 ± 1.8****	36.0 ± 1.5 ****	15.5 ± 1.1***	15.9 ± 1.9**	15.5 ± 1.7****	1.9 ± 0.3
D1	32.2 ± 1.2**	901.9 ± 6.5****	41.4 ± 1.7****	32.3 ± 0.9****	1.9 ± 0.4	2.6 ± 0.5	14.3 ± 2.8****	2.3 ± 1.2
D2	16.6 ± 0.1***	349.2 ± 3.5****	39.6 ± 2.1****	29.1 ± 2.7****	0.5 ± 0.1	0.7 ± 0.1	15.9 ± 2.3****	0.8 ± 0.01
D3	152.1 ± 4.5****	917.7 ± 4.6****	33.2 ± 1.1****	24.5 ± 1.8****	14.9 ± 1.6**	22.2 ± 1.6****	15.6 ± 2.4****	1.1 ± 0.2
D4	181.0 ± 1.4****	214.3 ± 2.6****	31.2 ± 0.8****	23.6 ± 0.5****	1.6 ± 0.8	2.9 ± 2.1	16.1 ± 2.3****	1.1 ± 0.1
A1b	143.4 ± 1.8****	858.1 ± 1.1****	9.8 ± 0.2****	8.4 ± 0.3****	8.4 ± 0.9*	12.7 ± 0.5****	102.2 ± 2.4****	0.2 ± 0.03****
A1c	146.0 ± 1.7****	341.3 ± 2.6****	9.3 ± 0.6****	7.1 ± 0.4****	10.7 ± 0.7***	15.8 ± 0.9****	60.4 ± 1.4	0.5 ± 0.07****
D2b	472.7 ± 3.7****	250.2 ± 3.5****	11.7 ± 1.1****	10.0 ± 0.8****	12.1 ± 0.7****	3.2 ± 0.4****	102.5 ± 2.2****	0.2 ± 0.01
D2c	42.9 ± 0.4****	15.3 %[#]	9.6 ± 0.6****	9.1 ± 0.3****	10.9 ± 0.4***	4.7 ± 0.6****	101.5 ± 3.0****	0.3 ± 0.03
Cornuside	5.8 ± 0.8	15.6 ± 1.3	8.4 ± 0.7	7.2 ± 0.6	20.8 ± 1.2	17.6 ± 1.1	103.0 ± 1.3	3.0 ± 0.3
Sweroside	0.9 ± 0.1	2.4 ± 0.3	8.3 ± 0.5	7.9 ± 0.8	NA	NA	NA	7.5 ± 0.5
Ellagic acid	2.7 ± 0.3	14.8 ± 1.2	NT	NT	2.5 ± 0.2	2.0 ± 0.1	102.7 ± 1.7	3.1 ± 0.3

Data are expressed as means ± S.D. ($n = 3$). A: *C. sanguinea* fresh leaves, B: *C. sanguinea* dried leaves; 1. Ethanol maceration; 2. Hydroalcoholic (60 %) maceration; 3. Decoction; 4. Ethanol ultrasound assisted extraction. C: *C. mas* fresh leaves; D: *C. mas* dried leaves. 1. Ethanol maceration; 2. Hydroalcoholic (60 %) maceration; 3. Decoction; 4. Ethanol ultrasound assisted extraction. A1b: ethanol maceration of *C. sanguinea* fresh leaves XAD-resin fraction 80 % EtOH; A1c: ethanol maceration of *C. sanguinea* fresh leaves XAD-resin fraction absolute EtOH. D2b: hydroalcoholic maceration of *C. mas* dried leaves XAD-resin fraction 80 % EtOH; D2c: hydroalcoholic maceration of *C. mas* dried leaves XAD-resin fraction absolute EtOH. Acarbose was used as positive control in α-amylase and α-glucosidase tests (IC_{50} of 35.5 ± 1.1 μg/mL against α-glucosidase, and IC_{50} of 50.0 ± 1.4 μg/mL against α-amylase). L-N6-(1-Iminoethyl)lysine was used as positive control in NO production test (IC_{50} of 1.0 ± 0.01 μg/mL). NA: not active; NT: not tested. Ascorbic acid (IC_{50} of 1.7 ± 0.2 μg/mL) was used as positive control in ABTS test. BHT (63.2 ± 4.3 μM Fe(II)/g) was used as positive control in FRAP test. Propyl gallate (IC_{50} of 1.0 ± 0.01 μg/mL after 30 and 60 min of incubation) was used as positive control in β-carotene bleaching test. Differences within and between groups were evaluated by One-way ANOVA followed by a multicomparison Dunnett's test (α = 0.05): ****$p < 0.0001$, ***$p < 0.001$, **$p < 0.01$, *$p < 0.1$ compared with the positive controls.

rules while fully satisfying the other filters. Despite its low membrane permeability, its pharmacokinetic profile supports further exploration.

Sweroside emerged as the most promising candidate regarding drug-likeness, demonstrating a balanced lipophilicity/solubility profile (consensus Log Po/w = −0.75). It exhibited moderate skin permeation (LogKp = −9.14) and a high bioavailability score (0.56).

Sweroside fully complied with Lipinski, and most other drug-likeness criteria, and showed high GI absorption, suggesting favourable oral bioavailability and metabolic stability.

In summary, the comprehensive ADMET and drug-likeness assessment confirms the therapeutic potential of all tested compounds. Among these, cornuside aglycone and sweroside emerge as particularly promising leads for future drug discovery efforts due to their optimal balance of solubility, lipophilicity, GI absorption, bioavailability, and compliance with drug-likeness parameters.

3.4. Cell viability and nitric oxide (NO) inhibition

The MTT assay results indicate that all *C. sanguinea* extracts reduced the viability of HFF-1 and RAW 264.7 cells only at the highest tested concentration (250 μg/mL) (Figs. S7 and S8, Supplementary Materials). At lower concentrations (2.5–12.5 μg/mL), fractions A1b and A1c

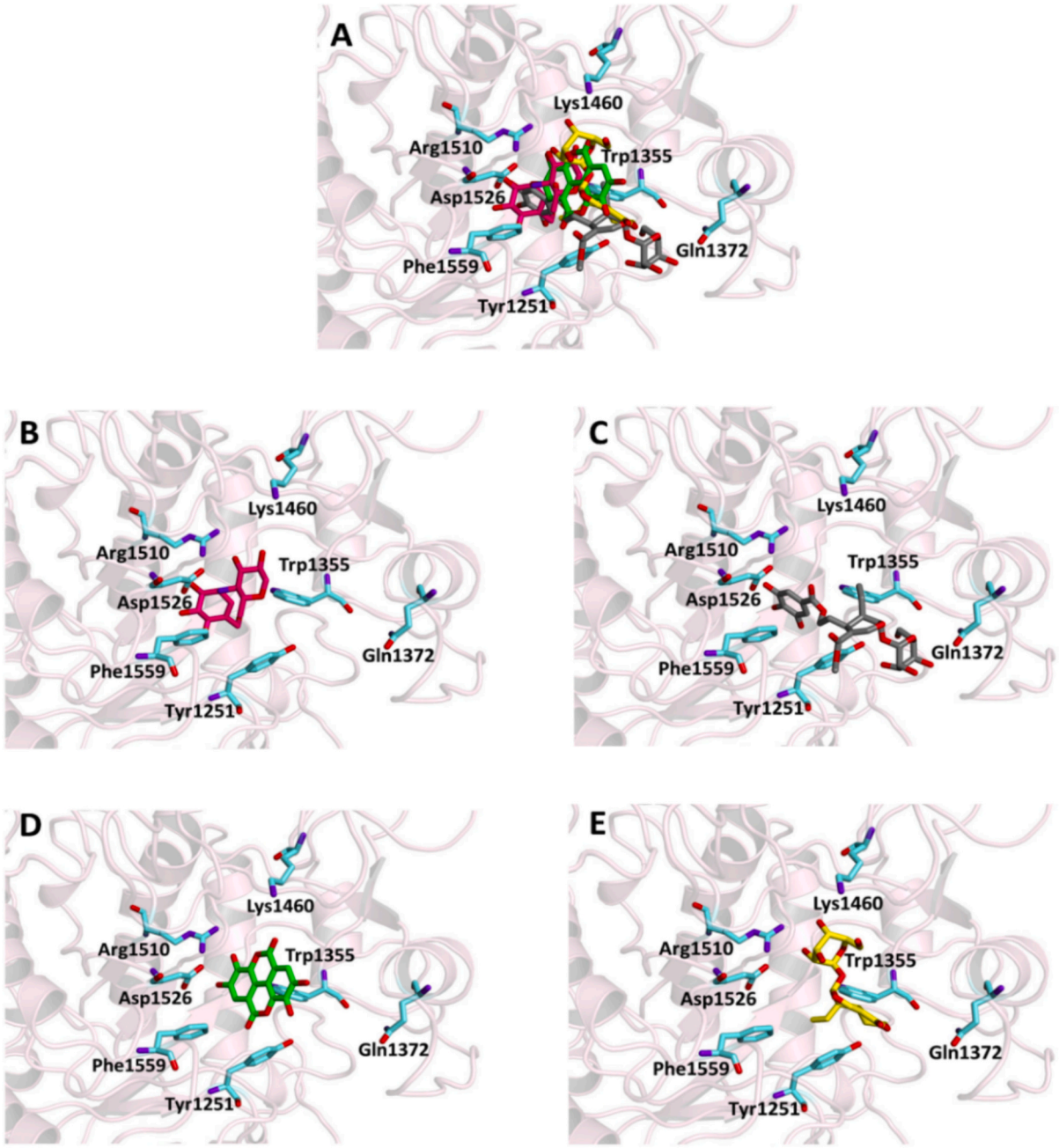

Fig. 1. Ligand-binding pocket of the active site of α-glucosidase. Protein backbone is represented in background as ribbons, and key protein residues are in cyan. (A) Superimposed binding modes of the crystallographic ligand acarbose (hotpink), cornuside (gray), ellagic acid (green) sweroside (yellow). The ligands are also shown separately: (B) acarbose, (C) cornuside, (D) ellagic acid and (E) sweroside. (For interpretation of the references to colour in this figure legend, the reader is referred to the web version of this article.)

enhanced cell viability in both HFF-1 and RAW 264.7 cells. Moreover, in HFF-1 cells, viability remained elevated even at 25 μg/mL, exceeding the levels observed in untreated controls. In contrast, at 250 μg/mL, both fractions exhibited cytotoxic effects, particularly A1c, which reduced cell viability by approximately 40 % in RAW 264.7 and by approximately 60 % in HFF-1 (Figs. S9 and S10, Supplementary Materials).

Regarding *C. mas*, extracts C1, C2, D3, and D4 reduced the viability of both HFF-1 and RAW 264.7 cells in a concentration-dependent manner across all tested concentrations. In contrast, C3 and D2 extracts exhibited cytotoxic effects only at the highest concentration (250 μg/mL), while C4 and D1 did not display any cytotoxicity at the tested doses (Figs. S7 and S8, Supplementary Materials).

Similarly, fractions D2b and D2c significantly reduced cell viability only at 250 μg/mL (Figs. S9 and S10, Supplementary Materials).

Cornuside showed cytotoxic effects in both cell lines at all concentrations tested (Figs. S9 and S10, Supplementary Materials). In contrast, sweroside and ellagic acid did not alter the viability of RAW 264.7 cells but significantly enhanced the viability of HFF-1 cells.

Several natural compounds have been shown to enhance the viability of HFF-1 cells, a human dermal fibroblast cell line commonly used in studies of skin physiology and wound healing. Different polyphenols, such as epigallocatechin gallate from *Camelia sinensis* and resveratrol from *Vitis vinifera* or curcumin from *Curcuma longa* have demonstrated significant cytoprotective and antioxidant properties, contributing to improved fibroblast survival, supporting cell viability, and collagen

Table 6
Chemical structures, complexes binding energy (BE) values, inhibition constant (Ki), Ligand Efficiency (LE) and key protein residues of α-glucosidase (3TOP) and α-amylase (4 W93) interacting with the ligands.

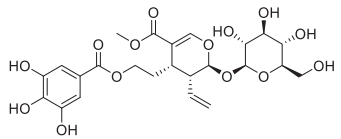

Cornuside

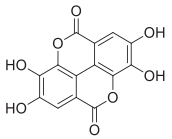

Ellagic acid

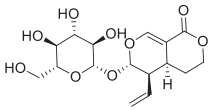

Sweroside

Ligand	3TOP								4 W93							
	BE kcal/mol	Ki μM	LE kcal/mol	Interactions					BE kcal/mol	Ki μM	LE kcal/mol	Interactions				
				Hydrogen Bonds				Hydrophobic Interaction Residues				Hydrogen Bonds				Hydrophobic Interaction Residues
				Residues	Distance Å		Donar Angle °					Residues	Distance Å		Donar Angle°	
					H-A	D-A							H-A	D-A		
Cornuside	−8.5	1.01	0.35	Tyr1251 Gln1372 Arg1377 Arg1510 Thr1586	2.10 2.07 2.81 2.45 3.17	2.99 2.94 3.43 2.99 4.09	151.32 148.04 121.56 114.55 158.83	Trp1355 Phe1559 Phe1560	−7.3	7.2	0.30	Asp197 Ala198 Ser199 Glu233 Ile235	2.13 3.49 3.61 1.96 1.83	3.06 3.92 4.03 2.88 2.80	158.97 108.93 108.51 158.22 168.88	Thr163 Ile235
Ellagic acid	−7.9	2.7	0.36	Asp1157 Trp1369 Arg1510 Asp1526	2.26 3.02 1.91 2.87	3.15 3.42 2.87 3.71	153.50 106.16 163.23 146.70	Phe1559 Trp1355 Phe1560	−7.9	2.7	0.36	Asp197 Ala198 Lys200 Ile235	3.33 2.91 2.17 2.57	3.69 3.38 3.06 3.36	104.53 109.71 145.77 136.71	Leu162 His200 Ile235 His201
Sweroside	−6.5	26.6	0.36	Lys1460 Asp1526	2.40 2.77	3.27 3.29	147.42 114.49	Tyr1251 Trp1355 Phe1559	−6.9	13.7	0.38	Arg195 Asp197 Ala198	3.08 3.04 3.36	4.03 3.84 4.03	163.79 139.87 126.61	Trp59 His305

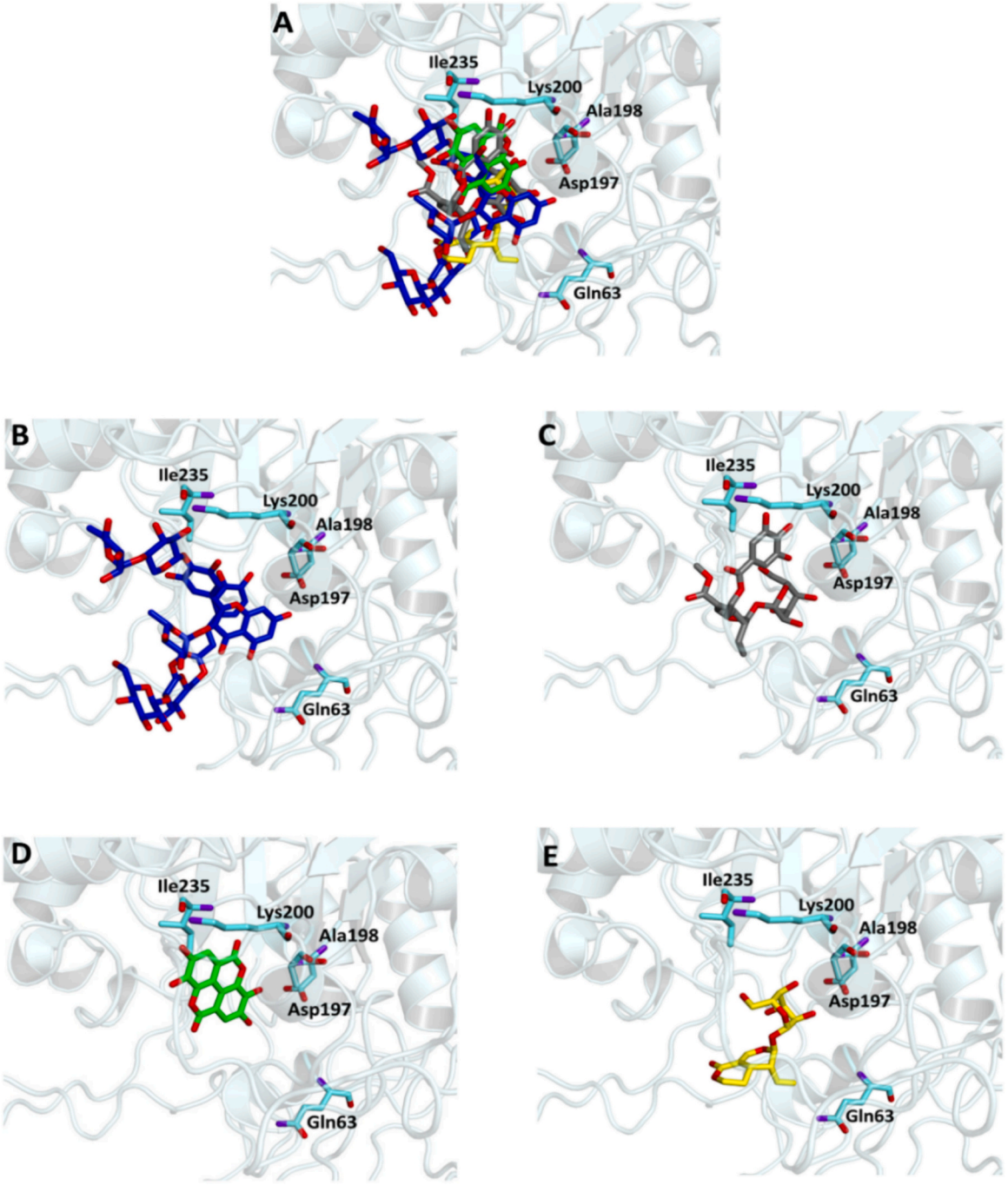

Fig. 2. Ligand-binding pocket of the active site of α-amylase. Protein backbone is represented in background as ribbons, and key protein residues are in cyan. (A) Superimposed binding modes of the crystallographic ligand montbretin A (blue), cornuside (gray), ellagic acid (green) sweroside (yellow). The ligands are also shown separately: (B) montbretin A, (C) cornuside, (D) ellagic acid and (E) sweroside. (For interpretation of the references to colour in this figure legend, the reader is referred to the web version of this article.)

production under stress conditions (Park et al., 2025; Tavakol et al., 2019; Xia et al., 2024). These findings suggest that natural compounds may serve as effective agents in dermatological and regenerative medicine for enhancing dermal cell health and potentially accelerating wound healing (Csekes & Račková, 2021).

Nitric oxide (NO), synthesized by the enzyme inducible nitric oxide synthase (iNOS), is a key signaling molecule involved in the inflammatory response (Brindisi et al., 2021). iNOS plays a central role in the pathogenesis of various inflammatory diseases, and its expression is markedly induced in macrophages upon stimulation with bacterial lipopolysaccharide (LPS) or the endogenous IL-1β, leading to the production of high levels of NO. In this study, the anti-inflammatory potential of Cornus leaf extracts, their respective fractions, and selected pure compounds was assessed using the Griess assay (Table 5). The extracts in RAW 264.7 cells, showed moderate inhibitory activity, with IC_{50} values ranging from 19.6 to 36.4 μg/mL.

Notably, the enriched fractions exhibited significantly improved activity, with IC_{50} values between 7.1 and 10.0 μg/mL; among them, fraction A1c was the most effective. Among the tested pure compounds, cornuside and sweroside displayed potent inhibitory effects on NO production, with IC_{50} values of 7.2 and 7.9 μg/mL, respectively. A comparable trend was observed in HFF-1 cells stimulated with IL-1β,

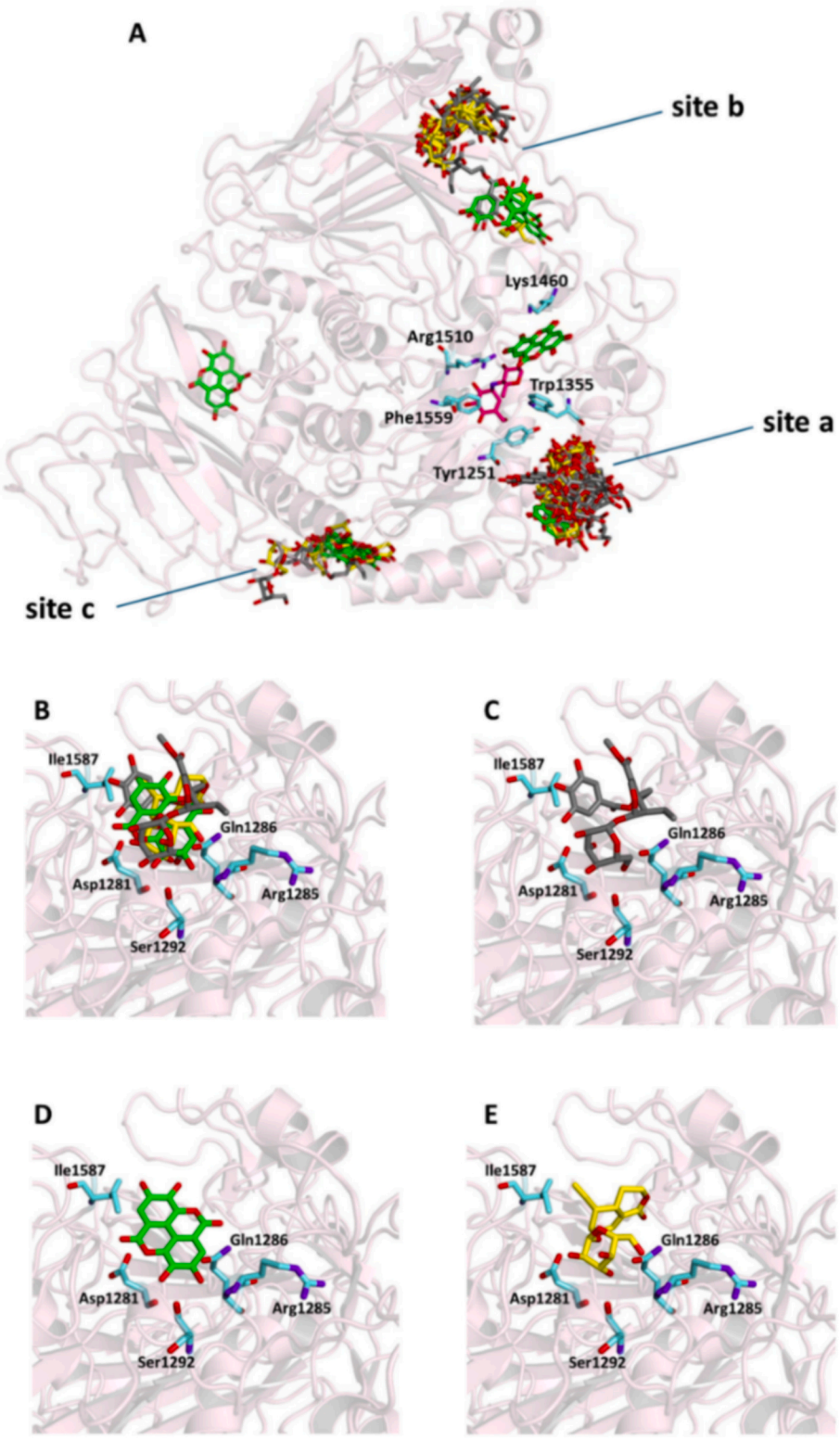

Fig. 3. (A) Hot-spots identified in the entire volume of α-glucosidase (3TOP) where compounds accommodate when the main active site is occupied. Protein backbone is represented in background as ribbons, and key protein residues are in cyan. (B) Superimposed binding modes of cornuside (gray), ellagic acid (green) and sweroside (yellow) in the most populated secondary site a. the ligands are also shown separately: (C) cornuside, (D) ellagic acid and (E) sweroside. (For interpretation of the references to colour in this figure legend, the reader is referred to the web version of this article.)

wherein the extracts exhibited a moderate protective effect, with effective concentrations ranging from 21.3 to 44.3 μg/mL. In contrast, both the fractions (9.3 to 11.7 μg/mL) and the pure compounds (8.4 and 8.3 μg/mL) demonstrated markedly higher efficacy (Table 5). These findings are consistent with previous reports indicating that cornuside reduces the expression of pro-inflammatory mediators such as TNF-α, IL-6, and NO in a dose-dependent manner in activated macrophages (Jiang et al., 2009; Kang et al., 2007). Similarly, sweroside has been shown to

Table 7
Complexes binding energy (BE) values, inhibition constant (Ki), Ligand Efficiency (LE) and key protein residues of the secondary site a of α-glucosidase (3TOP) and of α-amylase (4 W93) interacting with the ligands.

Ligand	site a 3TOP								site a 4 W93							
	BE kcal/mol	Ki μM	LE kcal/mol	Interactions				Hydrophobic Interaction Residues	BE kcal/mol	Ki μM	LE kcal/mol	Interactions				Hydrophobic Interaction Residues
				Hydrogen Bonds								Hydrogen Bonds				
				Residues	Distance Å		Donar Angle °					Residues	Distance Å		Donar Angle °	
					H-A	D-A							H-A	D-A		
Cornuside	−7.4	6.0	0.31	Gln1254	3.07	3.98	155.34	Arg1285	−7.0	11.8	0.30	Gly9	2.90	3.87	167.25	Phe335
				Asp1281	2.54	3.45	103.85	Val1363				Arg10	2.37	3.11	131.91	
				Arg1285	3.04	3.81	136.24	Ile1587				Thr11	2.28	2.78	110.84	
				Gln1286	2.02	2.96	160.44					Arg398	3.09	3.80	129.58	
				Ser1292	2.11	3.08	169.91					Asp402	2.00	2.96	167.72	
												Gly403	3.07	3.95	148.70	
Ellagic acid	−7.4	6.0	0.34	Asp1281	2.87	3.43	118.90	Ile1587	−8.1	2.0	0.37	Thr6	2.57	3.18	120.97	Thr11 Phe335
				Met1283	2.40	3.23	144.61					Ser289	3.05	3.55	114.13	
				Arg1285	2.41	3.36	163.79					Pro332	2.44	2.77	100.13	
				Gln1286	2.72	3.64	154.55					Gly334	2.67	3.14	110.17	
				Ser1292	2.18	3.05	148.03									
				Asp1357	2.77	3.10	101.38									
				Asp1281	2.89	3.77	158.48									
Sweroside	−7.8	3.2	0.43	Arg1285	2.72	3.37	123.95	Ile1587	−7.1	9.9	0.40	Thr6	2.52	3.17	124.65	Phe335
				Gln1286	2.46	3.19	131.11									
				Ser1292	2.98	3.79	140.94									

exert anti-inflammatory effects through inhibition of Nrf2, caspase-1, and IL-1β signaling pathways (Li et al., 2021).

The present findings highlight the therapeutic potential of polyphenol-rich natural extracts, particularly those from Cornus spp., in modulating inflammatory pathways relevant to skin disorders. The observed inhibitory effects on nitric oxide production in activated macrophages, coupled with the protective activity in IL-1β-stimulated HFF-1 fibroblasts, highlight the dual anti-inflammatory and cytoprotective properties of both the crude extracts and their bioactive fractions. Notably, the enhanced efficacy of purified compounds, such as cornuside and sweroside, suggests that targeted isolation of specific polyphenols may offer a more effective strategy for developing novel topical or systemic therapies for inflammatory skin conditions.

3.5. NF-κB inhibition

Nuclear factor-kappa B (NF-κB) is one of the ubiquitous eukaryotic transcription factors that regulate gene expression of cytokines and enzymes involved in controlling inflammatory responses. Recent studies have reported that NF-κB regulates the expression of inducible nitric oxide synthase (*i*NOS) and cyclooxygenase-2 (COX-2) (Guo et al., 2024). The activation of NF-κB is critically required for the activation of pro-inflammatory mediators in LPS-stimulated macrophages. Fraction A1b exerted a remarkable NO production inhibitory activity and interesting in vitro antioxidant effects. Considering these promising effects, fraction A1b was tested for its ability to reduce the activation of NF-κB in LPS-stimulated RAW 264.7 cells.

In particular, after the treatment of LPS-stimulated RAW 264.7 cells, the translocation of NF-κB into the nucleus was monitored. The results obtained highlighted the ability of this fraction to reduce the translocation of NF-κB into the nucleus (Fig. S11). The chemical analysis of this fraction revealed the presence of the seco-iridoid cornuside and the putative lignan cornuskoside A, together with galloyl derivatives and flavonoids (kaempferol derivatives, quercetin, and quercetin derivatives). Among these phytochemicals, quercetin and kaempferol has been found to possess potent anti-inflammatory effects, due in part to its anti-NF-κB activity (Das et al., 2024; Kadioglu et al., 2015; Nam, 2006). Li et al. (2023) showed as the seco-iridoid cornuside was able to reduce the translocation of activated NF-κB to the nucleus and inhibited the phosphorylation of IκB-α. Previously, cornuside showed anti-inflammatory activity in LPS-induced inflammation model via the inhibition of NF-κB activity (Choi et al., 2011). Moreover, Kang et al. (2007) observed that the addition of cornuside to human umbilical vein endothelial cell cultures reduced the mRNA expression of Vascular Cell Adhesion Molecule 1 (VCAM-1) and Intercellular Adhesion Molecule 1 (ICAM-1), and reduced the TNFα-induced NF-κB activation.

3.6. Antioxidant properties

Several studies have shown that diabetes mellitus is accompanied by decreased antioxidant capacity and increased formation of free radicals, leading to oxidative damage of cell structures (Akpoveso et al., 2023; Bashan et al., 2009). Therefore, the discovery of new molecules or extracts with hypoglycaemic properties and at the same time with antioxidant activity is desirable for diabetes prevention and treatment. In this work, the antioxidant activity was assessed by using different assays: ABTS test for the radical scavenging activity, FRAP test for the ability to reduce the complex of ferric ions (Fe^{3+})-ligand to ferrous complex (Fe^{2+}) and β-carotene bleaching test for the ability to prevent lipid oxidation. Data are reported in Table 5.

In ABTS test, except D1, all *C. mas* leaves extracts, exhibited high ability to scavenge the radical cation ABTS more than the positive control ascorbic acid. Among them, sample D2 resulted the most active (IC_{50} value of 0.8 μg/mL). This extract exhibited also the greater inhibition of lipid peroxidation with IC_{50} values of 0.49 and 0.70 μg/mL respectively after 30 and 60 min of incubation. A great $ABTS^{+\cdot}$ radical

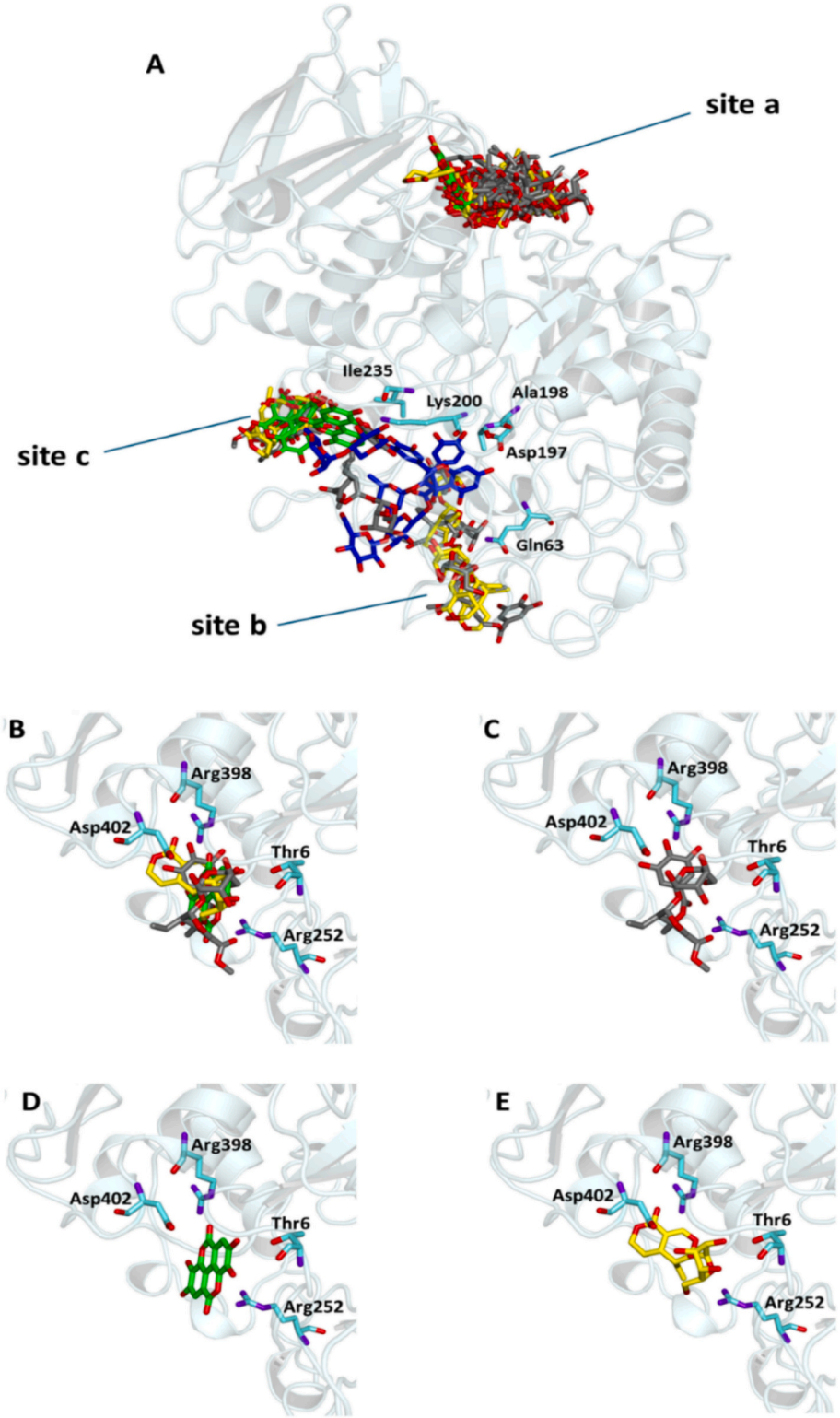

Fig. 4. (A) Hot-spots identified in the entire volume of α-amylase (4 W93) where compounds accommodate when the main active site is occupied. Protein backbone is represented in background as ribbons, and key protein residues are in cyan. (B) Superimposed binding modes of cornuside (gray), ellagic acid (green) and sweroside (yellow) in the most populated secondary site a. The ligands are also shown separately: (C) cornuside, (D) ellagic acid, and (E) sweroside. (For interpretation of the references to colour in this figure legend, the reader is referred to the web version of this article.)

cation ability was observed with *C. sanguinea* extracts with IC_{50} values ranging from 0.4 to 1.2 μg/mL, more than ascorbic acid (IC_{50} of 1.7 μg/mL). The same trend was observed in the FRAP test where all extracts presented a Fe^{3+}-reducing power better than BHT (63.20 μM Fe (II)/g), used as positive control, with values in the range 92.8–101.4 μM Fe (II)/g. Analysing results obtained in the lipid oxidation prevention, A1 extract exhibited the best results with IC_{50} values of 10.5 and 9.2 μg/mL, after 30 and 60 min of incubation, respectively.

The founded antioxidant activity of blood twig dogwood and cornelian cherry may be related to the different polyphenols detected in

Table 8
ADMET analysis of studied compounds using the SwissADME online server.

Compound	Solubility*				Lipophilicity** consensus Log $P_{o/w}$	Pharmacokinetics			Bioavailability Score	Drug likeness					Summary
	LogS (ESOL)	LogS (Ali)	LogS (SILICOS-IT)	S		GI absorption	BBB permeant	$LogK_p$ cm/s		Lipinski	Ghose	Veber	Egan	Muegge	
Cornuside	−2.46	−3.99	0.52	yes	−0.35 (low)	low	no	−9.76	0.11	3 violations	2 violations	2 violations	1 violation	3 violations	high polarity, low lipophilicity, poor membrane permeability and limited oral bioavailability expected.
Cornuside aglycone	−2.70	−3.98	−1.25	yes	1.15 (balanced)	high	yes	−7.64	0.56	yes	yes	1 violation	1 violation	yes	balanced lipophilicity, improved membrane permeability and oral bioavailability, favourable drug-likeness profile
Ellagic acid	−2.94	−3.66	−3.35	yes	1.00 (moderate)	high	yes	−7.36	0.55	yes	yes	1 violation	1 violation	yes	moderate lipophilicity, limited membrane permeability, but acceptable oral bioavailability and manageable drug-likeness
Sweroside	−1.22	−1.43	1.25	yes	−0.75 (balanced)	high	yes	−9.14	0.56	yes	1 violation	yes	1 violation	yes	balanced lipophilicity, good membrane permeability and high oral bioavailability, good drug-likeness profile

Note: S: soluble (logS > −4); **Lipophilicity is shown based on the average of all five Log P o/w predictions; **GI**: gastrointestinal; **BBB**: Blood-Brain Barrier; **$LogK_p$**: skin permeation of compounds.

the extracts, including gallic acid, ellagic acid, chlorogenic acid, quinic acid, syringic acid, and several flavonoids. These constituents have proven antioxidant properties and the ability to suppress specific enzymes engaged in intracellular ROS overproduction and to inhibit cell damage caused by free radicals (Kumar & Goel, 2019; Rice-Evans et al., 1995). In addition, literature data indicate that these molecules can inhibit lipid oxidation and have the ability to disorganize lipid chains (Pomianek et al., 2024). The antioxidant effects of tested *Cornus* extracts may also be the result of the action of iridoids, which can exert antioxidant effects through various mechanisms, including scavenging free radicals, modulating antioxidant enzyme activity, and inhibiting lipid peroxidation (Guo et al., 2025).

Few studies explored the antioxidant activity of *Cornus* leaves. The hydroalcoholic extract (80 % methanol) of cornelian cherry dried leaves showed an IC_{50} value of 165 μg/mL in the DPPH test and a percentage of inhibition of lipid peroxidation of 93 % at the concentration of 1 mg/mL in the β-carotene bleaching test (Celep et al., 2013). Successively, Stanković et al. (2014) explored the antioxidant activity of extracts of *C. mas* dried leaves obtained by methanol, water, ethyl acetate, acetone, and petroleum ether. The most interesting data were obtained by acetone and methanol extracts with IC_{50} values of 32.17 and 39.40 μg/mL, respectively, followed by water (IC_{50} of 59.28 μg/mL), petroleum ether (IC_{50} of 375.56 μg/mL) and ethyl acetate (IC_{50} of 381.34 μg/mL). To the best of our knowledge, this is the first report assessing the antioxidant activity of *C. sanguinea* leaf extracts.

The results obtained from the flavonoid-iridoid-enriched fractions are particularly noteworthy. A1b and D2b exerted the most promising antioxidant activity in both ABTS and FRAP tests. Moreover, in the β-carotene bleaching test A1b and D2b exhibited the best IC_{50} values of 8.4 μg/mL after 30 min of incubation and 3.2 μg/mL after 60 min of incubation, respectively. A1b fraction showed the presence of quercetin, quercetin derivatives, kaempferol derivatives, and cornuside. Sweroside, secologanin, cornuside, ellagic acid, gemin D, and several flavonoids such as rutin, quercetin, and kaempferol derivatives were identified in D2b fraction. Herein, we investigated the antioxidant potential of the pure compounds cornuside, sweroside and ellagic acid. In the β-carotene bleaching test, ellagic acid resulted the most active compound with IC_{50} values of 2.5 and 2.0 μg/mL, after 30 and 60 min of incubation, respectively. Cornuside and ellagic acid exerted a comparable antioxidant effect in both ABTS and FRAP tests. Sweroside showed activity exclusively in the ABTS assay, with an IC_{50} value of 7.5 μg/mL, and no activity was observed in the other assays. The antioxidant activity of the other constituents of the enriched fractions such as flavonoids is well known in literature. This activity is mainly due to their redox properties, which allow these phenolic compounds to act as hydrogen donators, reducing agents, and singlet oxygen quenchers. In addition, flavonoids have metal chelation potential effects (Rice-Evans et al., 1995).

4. Conclusion

In this study, we elucidated the chemical composition of different extracts of two *Cornus* species such as *Cornus mas* and *Cornus sanguinea* and their hypoglycaemic and antioxidant properties, as well as their anti-inflammatory activity (inhibition of NF-κB nuclear translocation and nitric oxide production). LC-ESI-QTOF-MS analysis led to the identification of phenolic acids, iridoids, and flavonoids as main classes of constituents found in *Cornus* extracts. Ethanol and hydroalcoholic maceration resulted the most promising procedure to obtain extracts characterized by the highest bioactivity primarily in terms of antioxidant and carbohydrate hydrolysing enzyme inhibition. In particular, ethanol maceration of fresh *C. sanguinea* leaves (A1 sample) and hydroalcoholic maceration of dried *C. mas* leaves (D2 sample) and exhibited the most promising bioactivity. Indeed, in order to obtain enriched fractions in flavonoids and iridoids, these extracts were subjected to fractionation by Amberlite XAD-16 resin. The obtained

fractions were tested to investigate their potential bioactivity together with three of the most representative constituents of both *Cornus* species, such as sweroside, cornuside, and ellagic acid. Sweroside exhibited a promising α-glucosidase and α-amylase inhibition. The comprehensive results of docking studies reveal compelling evidence that the main phytochemicals in Cornus extract effectively interact with critical residues in the active sites of both target proteins, as reflected in the calculated favourable binding energy and Ki values as well as a ligand efficiency higher than 0.30 kcal/mol, which is usually considered a promising indicator in early-stage drug discovery. In addition, the predicted ADMET (Absorption, Distribution, Metabolism, Excretion, and Toxicity) profiles were found to be compatible with drug-likeness criteria, further supporting their potential as bioactive candidates. Moreover, these studies have identified additional hot spots where compounds can bind when the primary active site is already occupied. These findings support the hypothesis that multiple compounds may simultaneously interact with the protein, explaining the enhanced activity of the entire extract compared to that of each single compound, as observed in biological experiments. Beyond confirming expected interactions, our docking analysis also provides novel exploratory insights into the pharmacological potential of the extract. Specifically, it highlights the possibility of simultaneous binding of different phytochemicals to distinct regions of the same protein, suggesting a synergistic effect that could underlie the extract's better bioactivity. This multi-site, multi-ligand interaction model reflects a more realistic scenario for complex botanical mixtures and helps explain their broader biological effects. Although these results are based on predictive computational models and in vitro assays, their strong convergence allows for a plausible mechanistic interpretation. The integration of molecular docking with biological data not only supports but also expands understanding of how phytochemicals in natural extracts exert their activity. Taken together, these findings highlight the value of in silico approaches in generating hypotheses that can guide further pharmacological investigations.

In conclusion, *C. mas* and *C. sanguinea* leaves could be considered good candidate for the extraction of phytocomplex/enriched fractions with a high potential for the prevention and treatment of chronic metabolic diseases such type 2 diabetes. Future research could explore the in vivo effects of the most promising *C. mas* and *C. sanguinea* extracts/fractions for evaluating their safety, toxicity, and efficacy.

CRediT authorship contribution statement

Maria Concetta Tenuta: Writing – review & editing, Writing – original draft, Investigation. **Brigitte Deguin:** Writing – review & editing, Writing – original draft, Methodology, Data curation, Conceptualization. **Monica Rosa Loizzo:** Writing – review & editing, Data curation. **Fedora Grande:** Writing – review & editing, Data curation. **Matteo Brindisi:** Investigation. **Maria Antonietta Occhiuzzi:** Investigation. **Annabelle Dugay:** Writing – original draft, Investigation. **Marco Bonesi:** Writing – review & editing, Investigation. **Giuseppe Antonio Malfa:** Writing – review & editing, Investigation. **Rosa Tundis:** Writing – original draft, Methodology, Data curation, Conceptualization.

Declaration of competing interest

The authors declare that they have no known competing financial interests or personal relationships that could have appeared to influence the work reported in this paper.

Acknowledgements

Authors thank Dr. N.G. Passalacqua for the botanical identification of *C. mas* and *C. sanguinea* leaves and thank POS CAL.HUB.RIA project funded by the Italian Minister of Health (CUP H53C22000800006) for the financial support to M.A. Occhiuzzi.

Appendix A. Supplementary data

Supplementary data to this article can be found online at https://doi.org/10.1016/j.jff.2025.107002.

Data availability

Data will be made available on request.

References

Adasme, M. F., Linnemann, K. L., Bolz, S. N., Kaiser, F., Salentin, S., Haupt, V. J., & Schroeder, M. (2021). PLIP 2021: Expanding the scope of the protein-ligand interaction profiler to DNA and RNA. *Nucleic Acids Research, 49*, W530–W534.

Akpoveso, O.-O. P., Ubah, E. E., & Obasanmi, G. (2023). Antioxidant phytochemicals as potential therapy for diabetic complications. *Antioxidants, 12*, 123.

Badalica-Petrescu, M., Dragan, S., Ranga, F., Fetca, F., & Socaciu, C. (2014). Comparative HPLC-DAD-ESI (+) MS fingerprint and quantification of phenolic and flavonoid composition of aqueous leaf extracts of *Cornus mas* and *Crataegus monogyna* in relation to their cardiotonic potential. *Notulae Botanicae Horti Agrobotanici, 42*, 9–18.

Bashan, N., Kovsan, J., Kachko, I., Ovadia, H., & Rudich, A. (2009). Positive and negative regulation of insulin signaling by reactive oxygen and nitrogen species. *Physiological Reviews, 89*, 27–71.

Bhattachartya, S., Christensen, K. B., Olsen, L. C., Christensen, L. P., Grevsen, K., Faergeneman, N. J., Kristiansen, K., Young, J. F., & Oksbejerq, N. (2013). Bioactive components from flowers of *Sambucus nigra* L. increase glucose uptake in primary porcine myotube cultures and reduce fat accumulation in *Caenorhabditis elegans*. *Journal of Agricultural and Food Chemistry, 61*, 11033–11040.

Bimakr, M., Rahman, R. A., Taip, F. S., Ganjloo, A., Salleh, L. M., Selamat, J., Hamid, A., & Zaidul, I. S. M. (2011). Comparison of different extraction methods for the extraction of major bioactive flavonoid compounds from spearmint (*Mentha spicata* L.) leaves. *Food and Bioproducts Processing, 89*, 67–72.

Bourquelot, E., & Herissey, H. C. R. (1902). *Academy of Sciences, 134*, 1441–1443.

Brindisi, M., Bouzidi, C., Frattaruolo, L., Loizzo, M. R., Cappello, M. S., Dugay, A., Deguin, B., Lauria, G., Cappello, A. R., & Tundis, R. (2021). New insights into the antioxidant and anti-inflammatory effects of Italian Salvia officinalis leaf and flower extracts in lipopolysaccharide and tumor-mediated inflammation models. *Antioxidants, 10*, 311.

Cai, H., Cao, G., & Cai, B. (2013). Rapid simultaneous identification and determination of the multiple compounds in crude fructus Corni and its processed products by HPLC-MS/MS with multiple reaction monitoring mode. *Pharmaceutical Biology, 51*, 273–278.

Celep, E., Aydın, A., Kırmızıbekmez, H., & Yesilada, E. (2013). Appraisal of *in vitro* and *in vivo* antioxidant activity potential of cornelian cherry leaves. *Food and Chemical Toxicology, 62*, 448–455.

Chen, C., Chaudhary, A., & Mathys, A. (2020). Nutritional and environmental losses embedded in global food waste. *Resources, Conservation and Recycling, 160*, Article 104912.

Choi, Y. H., Jin, G. Y., Li, G. Z., & Yan, G. H. (2011). Cornuside suppresses lipopolysaccharide-induced inflammatory mediators by inhibiting nuclear factor-κ B activation in RAW 264.7 macrophages. *Biological and Pharmaceutical Bulletin, 34*, 959–966.

Cirillo, F., Spinelli, A., Talia, M., Scordamaglia, D., Santolla, M. F., Grande, F., Rizzuti, B., Maggiolini, M., Gérard, C., & Lappano, R. (2024). Estetrol/GPER/SERPINB2 transduction signaling inhibits the motility of triple-negative breast cancer cells. *Journal of Translational Medicine, 22*, 450.

Cook, S. D. (2019). An historical review of phenylacetic acid. *Plant and Cell Physiology, 60*, 243–254.

Cory, H., Passarelli, S., Szeto, J., Tamez, M., & Mattei, J. (2018). The role of polyphenols in human health and food systems: A mini-review. *Frontiers in Nutrition, 5*, 87.

Csekes, E., & Račková, L. (2021). Skin aging, cellular senescence and natural polyphenols. *International Journal of Molecular Sciences, 22*, 12641.

Das, D., Banerjee, A., Mukherjee, S., & Maji, B. K. (2024). Quercetin inhibits NF-kB and JAK/STAT signaling via modulating TLR in thymocytes and splenocytes during MSG-induced immunotoxicity: An in vitro approach. *Molecular Biology Reports, 51*, 277–290.

Davì, F., Taviano, M. F., Acquaviva, R., Malfa, G. A., Cavò, E., Arena, P., Ragusa, S., Cacciola, F., El Majdoub, Y. O., Mondello, L., & Miceli, N. (2023). Chemical profile, antioxidant and cytotoxic activity of a phenolic-rich fraction from the leaves of *Brassica fruticulosa* subsp. *fruticulosa* (Brassicaceae) growing wild in Sicily (Italy). *Molecules, 28*, 2281.

De Luca, M., Occhiuzzi, M. A., Rizzuti, B., Ioele, G., Ragno, G., Garofalo, A., & Grande, F. (2022). Interaction of letrozole and its degradation products with aromatase: Chemometric assessment of kinetics and structure-based binding validation. *Journal of Enzyme Inhibition and Medicinal Chemistry, 37*, 1600–1609.

Deng, S., West, B. J., & Jensen, C. J. (2013). UPLC-TOF-MS characterization and identification of bioactive iridoids in *Cornus mas* fruit. *Journal of Analytical Methods in Chemistry*, Article 710972.

Dinda, B., Kyriakopoulos, A. M., Dinda, S., Zoumpourlis, V., Thomaidis, N. S., Velegraki, A., Markopoulos, C., & Dinda, M. (2016). *Cornus mas* L. (cornelian cherry), an important European and Asian traditional food and medicine: Ethnomedicine, phytochemistry and pharmacology for its commercial utilization in drug industry. *Journal of Ethnopharmacology, 193*, 670–690.

Drkenda, P., Spahic, A., Begic-Akagic, A., Gasi, F., Vranac, A., Hudina, M., & Blanke, M. (2014). Pomological characteristics of some autochthonous genotypes of cornelian cherry (*Cornus mas* L.) in Bosnia and Herzegovina. *Erwerbs-Obstbau, 56*, 59–66.

Durazzo, A., Caiazzo, E., Lucarini, M., Cicala, C., Izzo, A. A., Novellino, E., … Santini, A. (2019). Polyphenols: A concise overview on the chemistry, occurrence, and human health. *Phytotherapy Research, 33*, 2221–2243.

Eurostat. (2023). https://food.ec.europa.eu/safety/food-waste_en#about-food-waste.

Fredsgaard, M., Tchoumtchoua, J., Kohnen, S., Chaturvedi, T., & Thomsen, M. H. (2023). Isolation of polyphenols from aqueous extract of the halophyte *Salicornia ramosissima*. *Molecules, 31*, 220.

Grande, F., Occhiuzzi, M. A., Perri, M. R., Ioele, G., Rizzuti, B., Statti, G., & Garofalo, A. (2021). Polyphenols from *Citrus* Tacle® extract endowed with HMGCR inhibitory activity: An antihypercholesterolemia natural remedy. *Molecules, 26*, 5718.

Guendouze-Bouchefa, N., Madani, K., Chibane, M., Boulekbache-Makhlouf, L., Hauchard, D., Kiendrebeogo, M., Stévigny, C., Okusa, P. N., & Duez, P. (2015). Phenolic compounds, antioxidant and antibacterial activities of three Ericaceae from Algeria. *Industrial Crops and Products, 70*, 459–466.

Guo, L., Qiao, J., Junwei Huo, J., & Rupasinghe, H. P. V. (2025). Plant iridoids: Chemistry, dietary sources and potential health benefits. *Food Chemistry: X, 27*, Article 102491.

Guo, Q., Jin, Y., Chen, X., Ye, X., Shen, X., Lin, M., … Zhang, J. (2024). NF-κB in biology and targeted therapy: New insights and translational implications. *Signal Transduction and Targeted Therapy, 9*, 1–37.

Guo, X., Li, K., Guo, A., & Li, E. (2020). Intestinal absorption and distribution of naringin, hesperidin, and their metabolites in mice. *Journal of Functional Foods, 74*, Article 104158.

Guzhva, N. N. (2008). Coumarins from *Astragalus asper*. *Chemistry of Natural Compounds, 44*, 6.

Hanwell, M. D., Curtis, D. E., Lonie, D. C., Vandermeerschd, T., Zurek, E., & Hutchison, G. R. (2012). Avogadro: An advanced semantic chemical editor, visualization, and analysis platform. *Journal of Cheminformatics, 4*, 1–17.

Hatano, T., Ogawa, N., Kira, R., Yasuhara, T., & Okuda, T. (1989). Tannins of Cornaceous plants. I. Cornusiins A, B and C, dimeric monomeric and trimeric hydrolyzable tannins from *Cornus officinalis*, and orientation of valoneoyl group in related tannins. *Chemical and Pharmaceutical Bulletin, 37*, 2083–2090.

Hobbs, C. A., Swartz, C., Maronpot, R., Davis, J., Recio, L., Koyanagi, M., & Hayashi, S. M. (2015). Genotoxicity evaluation of the flavonoid, myricitrin, and its aglycone, myricetin. *Food Chemistry and Toxicology, 83*, 283–292.

Hozoori, Z., Pashna, Z., Yousfbeyk, F., & Amin, G. (2012). Evaluation of antioxidant activities of methanolic extract of Cornus sanguinea subsp. australis fruits. *Research in Pharmaceutical Sciences, 7*, S790.

Humphrey, W., Dalke, A., & Schulten, K. (1996). VMD: Visual molecular dynamics. *Journal of Molecular Graphics, 14*, 33–38.

Iannuzzi, A. M., Giacomelli, C., De Leo, M., Russo, L., Camangi, F., De Tommasi, N., … Trincavelli, M. L. (2021). *Cornus sanguinea* fruits: A source of antioxidant and antisenescence compounds acting on aged human dermal and gingival fibroblasts. *Planta Medica, 87*, 879–891.

Jiang, W. L., Chen, X. G., Zhu, H. B., & Tian, J. W. (2009). Effect of cornuside on experimental sepsis. *Planta Medica, 75*, 614–619.

Kadioglu, O., Nass, J., Saeed, M. E. M., Schuler, B., & Efferth, T. (2015). Kaempferol is an anti-inflammatory compound with activity towards NF-κB pathway proteins. *Anticancer Research, 35*, 2645–2650.

Kandar, C. C. (2021). Secondary metabolites from plant sources. *Bioactive Natural Products for Pharmaceutical Applications*, 329–377.

Kang, D. G., Moon, M. K., Lee, A. S., Kwon, T. O., Kim, J. S., Lee, H. S., & H.S.. (2007). Cornuside suppresses cytokine-induced proinflammatory and adhesion molecules in the human umbilical vein endothelial cells. *Biological and Pharmaceutical Bulletin, 30*, 1796–1799.

Kenny, P. W. (2019). The nature of ligand efficiency. *Journal of Cheminformatics, 11*, Article 8.

Korulkina, L. M., Shults, E. E., Zhusupova, G. E., Abilov, Z. A., Erzhanov, K. B., & Chaudri, M. I. (2004). Biologically active compounds from *Limonium gmelinii* and *L. Popovii* I. *Chemistry of Natural Compounds, 40*, 465–471.

Krivoruchko, E. V. (2014). Carboxylic acids from *Cornus mas*. *Chemistry of Natural Compounds, 50*, 112–113.

Kumar, N., & Goel, N. (2019). Phenolic acids: Natural versatile molecules with promising therapeutic applications. *Biotechnology Reports, 24*, E00370.

Lee, D., Kang, S-J., Lee, S-H., Ro, J., Lee, K., Kinghorn, A.D. (2000). Phenolic compounds from the leaves of *Cornus controversa*. Phytochemistry, 53, 405–407.

Lee, D. Y., Yoo, K. H., Chung, I. S., Kim, J. Y., Chung, D. K., Kim, D. K., … Baek, N. I. (2008). A new lignan glycoside from the fruits of *Cornus kousa* burg. *Archives of Pharmacal Research, 31*, 830.

Lee, J., Jang, D. S., Kim, N. H., Lee, Y. M., Kim, J., & Kim, J. S. (2011). Galloyl glucoses from the seeds of *Cornus officinalis* with inhibitory activity against protein glycation, aldose reductase, and cataractogenesis ex *vivo*. *Biological and Pharmaceutical Bulletin, 34*, 443–446.

Lee, S.H., Tanaka, T., Nonaka, G-I., Nishioka, I. (1989). Sedoheptulose digallate from *Cornus officinalis*. Phytochemistry, 28, 3469–3472.

Lee, S. W., Kim, H., & Ahn, J. H. (2021). Biosynthesis of ethyl caffeate via caffeoyl-CoA acyltransferase expression in *Escherichia coli*. *Applied Biological Chemistry, 64*, 1–6.

Li, J., Zhao, C., Zhu, Q., Wang, Y., Li, G., Li, X., Li, Y., Wu, N., & Ma, C. (2021). Sweroside protects against myocardial ischemia-reperfusion injury by inhibiting oxidative stress and pyroptosis partially via modulation of the keap1/Nrf2 axis. *Frontiers in Cardiovascular Medicine, 19*, Article 650368.

Li, S. S., Wu, J., Chen, L. G., Du, H., Xu, Y. J., Wang, L. J., Zhang, H. J., Zheng, X. C., & Wang, L. S. (2014). Biogenesis of C-glycosyl flavones and profiling of flavonoid glycosides in lotus (*Nelumbo nucifera*). *PLoS One, 9*, Article e108860.

Li, X., Guo, L., Huang, F., Xu, W., & Peng, G. (2023). Cornuside inhibits glucose-induced proliferation and inflammatory response of mesangial cells. *Korean Journal of Physiology & Pharmacology, 27*, 513–520.

Lidiková, J., Čeryová, N., Grygorieva, O., Bobková, A., Bobko, M., Árvay, J., Šnirc, M., Brindza, J., Ňorbová, M., Harangozo, L., & Kňazovická, V. (2024). Cornelian cherry (*Cornus mas* L.) as a promising source of antioxidant phenolic substances and minerals. *European Food Research and Technology, 250*, 1745–1754.

Lipinski, C. A. (2004). Lead- and drug-like compounds: The rule-of-five revolution. *Drug Discovery Today: Technologies, 1*, 337–341.

Loizzo, M. R., Bonesi, M., Menichini, F., Tenuta, M. C., Leporini, M., & Tundis, R. (2016). Antioxidant and carbohydrate-hydrolysing enzymes potential of *Sechium edule* (Jacq.) Swartz (Cucurbitaceae) peel, leaves and pulp fresh and processed. *Plant Foods for Human Nutrition, 71*, 381–387.

Lotfi, M., Keshvari, T., Taghizadeh, M. S., Afsharifar, A., Moghadam, A., Aram, F., & Niazi, A. (2025). Optimizing *Camelina sativa* oil extraction and its cytotoxicity using RSM by emphasis on antioxidant properties, physical characteristics, and molecular docking insights. *Industrial Crops and Products, 224*, Article 120334.

Malhotra, S., & Misra, K. (1981). Ellagic acid 4-*O*-rutinoside from pods of *Prosopis juliflora*. *Phytochemistry, 20*, 2439–2440.

Mark, R., Lyu, X., Lee, J. J. L., Parra-Saldívar, R., Chen, W. N., & W.N.. (2019). Sustainable production of natural phenolics for functional food applications. *Journal of Functional Foods, 57*, 233–254.

Meringolo, L., Bonesi, M., Sicari, V., Rovito, S., Passalacqua, N. G., Loizzo, M. R., & Tundis, R. (2022). Essential oils and extracts of *Juniperus macrocarpa* Sm. And *Juniperus oxycedrus* L.: Comparative phytochemical composition and anti-proliferative and antioxidant activities. *Plants, 11*, 1025–1043.

Messinese, E., Pitirollo, O., Grimaldi, M., Milanese, D., Sciancalepore, C., & Cavazza, A. (2024). By-products as sustainable source of bioactive compounds for potential application in the field of food and new materials for packaging development. *Food and Bioprocess Technology, 17*, 606–627.

Morris, G. M., Goodsell, D. S., Halliday, R. S., Huey, R., Hart, W. E., Belew, R. K., & Olson, A. J. (1998). Automated docking using a lamarckian genetic algorithm and an empirical binding free energy function. *Journal of Computational Chemistry, 1998* (19), 1639–1662.

Nam, N. H. (2006). Naturally occurring NF-kappaB inhibitors. *Mini Reviews in Medicinal Chemistry, 6*, 945–951.

Park, J. H., Jeong, E. Y., Kim, Y. H., Cha, S. Y., Kim, H. Y., Nam, Y. K., Park, J. S., Kim, S. Y., Lee, Y. J., Yoon, J. H., So, B., Kim, D., Kim, M., Byun, Y., Lee, Y. H., Shin, S. S., & Park, J. T. (2025). Epigallocatechin gallate in *Camellia sinensis* ameliorates skin aging by reducing mitochondrial ROS production. *Pharmaceuticals, 23*, 612.

Pawlowska, A. M., Camangi, F., & Braca, A. (2010). Quali-quantitative analysis of flavonoids of *Cornus mas* L. (Cornaceae) fruits. *Food Chemistry, 119*, 1257–1261.

Pomianek, T., Zagórska-Dziok, M., Skóra, B., Ziemlewska, A., Nizioł-Łukaszewska, Z., Wójciak, M., Sowa, I., & Szychowski, K. A. (2024). Comparison of the antioxidant and cytoprotective properties of extracts from different cultivars of *Cornus mas* L. *International Journal of Molecular Sciences, 25*, 5495.

Popović, Z., Bajić-Ljubičić, J., Matić, R., & Bojović, S. (2017). First evidence and quantification of quercetin derivatives in dogberries (*Cornus sanguinea* L.). *Turkish Journal of Biochemistry, 42*, 513–518.

Rahman, M. M., Rahaman, M. S., Islam, M. R., Rahman, F., Mithi, F. M., Alqahtani, T., … Uddin, S. (2022). Role of phenolic compounds in human disease: Current knowledge and future prospects. *Molecules, 27*, 233–269.

Ren, L., Qin, X., Cao, X., Wang, L., Bai, F., Bai, G., & Shen, Y. (2011). Structural insight into substrate specificity of human intestinal maltase-glucoamylase. *Protein & Cell, 2*, 827–836.

Rice-Evans, C.-A., Miller, N. J., Bolwell, P. G., Bramley, P. M., & Pridham, J. B. (1995). The relative antioxidant activities of plant-derived polyphenolic flavonoids. *Free Radical Research, 22*, 375–383.

Seif Zadeh, N., & Zeppa, G. (2022). Recovery and concentration of polyphenols from roasted hazelnut skin extract using macroporous resins. *Foods, 11*, 1969.

Sevindik, M., Khassanov, V. T., Sevindik, E., Uysal, I., & Mohammed, F. S. (2024). Cornelian cherry (*Cornus mas* L.): A comprehensive review on its usage areas, biological activities, mineral, phenolic and chemical contents and applications. *Applied Fruit Science, 66*, 2061–2071.

Shahraki, Z., Taghizadeh, M. S., Niazi, A., Rowshan, V., & Moghadam, A. (2024). Enhancing bioactive compound production in Salvia mirzayanii through elicitor application: Insights from in vitro and in silico studies. *Food Bioscience, 60*, Article 104185.

Shen, L., Pang, S., Zhong, M., Sun, Y., Qayum, A., Liu, Y., Rashid, A., Xu, B., Liang, Q., Ma, H., & Xiaofeng Ren, X. (2023). A comprehensive review of ultrasonic assisted extraction (UAE) for bioactive components: Principles, advantages, equipment, and combined technologies. *Ultrasonics Sonochemistry, 101*, Article 106646.

Sochor, J., Jurikova, T., Ercisli, S., Mlcek, J., Baron, M., Balla, S., Yilmaz, S. O., & Necas, T. (2014). Characterization of cornelian cherry (*Cornus mas* L.) genotypes-genetic resources for food production in Czech Republic. *Genetika, 46*, 915–924.

Stanković, M. S., & Topuzović, M. D. (2012). *In vitro* antioxidant activity of extracts from leaves and fruits of common dogwood (*Cornus sanguinea* L.). *Acta Botanica Gallica, 159*, 79–83.

Stanković, M. S., Zia-Ul-Haq, M., Bojovic, B. M., & Topuzovic, M. D. (2014). Total phenolics, flavonoid content and antioxidant power of leaf, flower and fruits from cornelian cherry (Cornus mas L.). *Bulgarian Journal of Agricultural Science, 20*, 358–363.

Szczepaniak, O. M., Kobus-Cisowska, J., Kusek, W., & Przeor, M. (2019). Functional properties of cornelian cherry (*Cornus mas* L.): A comprehensive review. *European Food Research and Technology, 245*, 2071–2087.

Taghizadeh, M. S., Niazi, A., Moghadam, A., & Afsharifar, A. (2022). Experimental, molecular docking and molecular dynamic studies of natural products targeting overexpressed receptors in breast cancer. *PLoS One, 17*, Article e0267961.

Tanaka, N., Tanaka, T., Fujioka, T., Fujii, H., Mihashi, K., Shimomura, K., & Ishimaru, K. (2001). An ellagic compound and iridoids from *Cornus capitata* root cultures. *Phytochemistry, 57*, 1287–1291.

Tavakol, S., Zare, S., Hoveizi, E., Tavakol, B., & Rezayat, S. M. (2019). The impact of the particle size of curcumin nanocarriers and the ethanol on beta_1-integrin overexpression in fibroblasts: A regenerative pharmaceutical approach in skin repair and anti-aging formulations. *Daru, 27*, 159–168.

Tenuta, M. C., Deguin, B., Loizzo, M. R., Cuyamendous, C., Bonesi, M., Sicari, V., Trabalzini, L., Mitaine-Offer, A.-C., Xiao, J., & Tundis, R. (2022). An overview of traditional uses, phytochemical compositions and biological activities of edible fruits of European and Asian *Cornus* species. *Foods, 11*, 1240.

Tenuta, M. C., Malfa, G. A., Bonesi, M., Acquaviva, R., Loizzo, M. R., Dugay, A., … Deguin, B. (2020). LC-ESI-QTOF-MS profiling, protective effects on oxidative damage, and inhibitory activity of enzymes linked to type 2 diabetes and nitric oxide production of *Vaccinium corymbosum* L. (Ericaceae) extracts. *Journal of Berry Research, 10*, 603–622.

Tomás-Barberán, F. A., Amparo Blázquez, M., Garcia-Viguera, C., Ferreres, F., & Tomás-Lorente, F. (1992). A comparative study of different amberlite XAD resins in flavonoid analysis. *Phytochemical Analysis, 3*, 178–181.

Trott, O., & Olson, A. J. (2010). AutoDock Vina: Improving the speed and accuracy of docking with a new scoring function, efficient optimization, and multithreading. *Journal of Computational Chemistry, 31*, 455–461.

Tundis, R., Grande, F., Occhiuzzi, M. A., Sicari, V., Loizzo, M. R., & Cappello, A. R. (2023). *Lavandula angustifolia* mill. (Lamiaceae) ethanol extract and its main constituents as promising agents for the treatment of metabolic disorders: Chemical profile, *in vitro* biological studies, and molecular docking. *Journal of Enzyme Inhibition and Medicinal Chemistry, 38*, 2269481.

Wang, C., Gong, X., Bo, A., Zhang, L., Zhang, M., Zang, E., … Li, M. (2020). Iridoids: Research advances in their phytochemistry, biological activities, and pharmacokinetics. *Molecules, 25*, 287–311.

Waszkowiak, K., & Gliszczynska-Swigło, A. (2016). Binary ethanol-water solvents affect phenolic profile and antioxidant capacity of flaxseed extracts. *European Food Research Technology, 242*, 777–786.

Williams, L. K., Zhang, X., Caner, S., Tysoe, C., Nguyen, N. T., Wicki, J., Williams, D. E., Coleman, J., McNeill, J. H., Yuen, V., Andersen, R. J., Withers, S. G., & Brayer, G. D. (2015). The amylase inhibitor montbretin A reveals a new glycosidase inhibition motif. *Nature Chemical Biology, 11*, 691–696.

Xia, Y., Zhang, H., Wu, X., Xu, Y., & Tan, Q. (2024). Resveratrol activates autophagy and protects from UVA-induced photoaging in human skin fibroblasts and the skin of male mice by regulating the AMPK pathway. *Biogerontology, 25*, 649–664.

Yadav, S., Malik, K., Moore, J. M., Kamboj, B. R., Malik, S., Malik, V. K., … Bishnoi, D. K. (2024). Valorisation of Agri-food waste for bioactive compounds: Recent trends and future sustainable challenges. *Molecules, 29*, 2055.

Yan, X., Murphy, B. T., Hammond, G. B., Vinson, J. A., & Neto, C. C. (2002). Antioxidant activities and antitumor screening of extracts from cranberry fruit (*Vaccinium macrocarpon*). *Journal of Agricultural and Food Chemistry, 50*, 5844–5849.